communications biology

A Nature Portfolio journal

Article

https://doi.org/10.1038/s42003-025-08667-8

Evaluating in-vivo spontaneous firing rate in the brain based on neuronal noise modeling

Hila Dvir [1,5] ✉, Shu Guo [2,5] ✉, Rui Kang [3,4], Daqing Li [3] & Shlomo Havlin [1]

Even without external stimuli, neurons produce spontaneous bursts of activities. Theoretical and practical clinical considerations, suggest the importance of determining the in-vivo statistical profile of those spontaneous spikes bursts, however this task has not been accomplished yet. Currently, it is only accepted that the in-vivo value of the mean firing rate (λ) of those spontaneous bursts is below 0.1Hz, without knowing its specific value and its population distribution. Here we propose a framework to evaluate the neurons' λ during rest of a given subject, using stochastic signal processing analysis of in-vivo brain fMRI and EEG. Our main hypothesis is that during rest the input to the neurons is mostly formed by a random neuronal noise, and although it fluctuates with zero mean, it affects the neurons' signal output characteristics. Our results based on in-vivo human fMRI and EEG databases, suggest that different people have different and stable characteristic λ values, and that λ of different functional systems of the same subject correlate in their values. Moreover, we find here that the λ values of subjects correlate with their brain task performances, in particular for tasks which are known to be affected by changes in neuronal noise or neuronal excitability threshold.

The neuronal voltage and current at rest fluctuate due to the stochastic behavior of the individual ion channel, which is the neuronal most basic electronic element. This stochastic dynamic occasionally leads to spontaneous action potentials even without any stimulation, a trait that has diverse effects on human physiology, and therefore captured the attention of many researchers from different scientific disciplines[1–7]. For example, the stochastic activity of the neurons is considered as the major reason for the resting brain to consume large amount of energy[1]. Therefore, in an effort to estimate the in-vivo average firing rate of resting brain, some studies use energy economy calculations, and vice versa estimating general resting brain energy from global rough estimations of mean firing rate[8].

Since spontaneous firing of spikes accounts for most of the total brain metabolic energy (between 60% and 80%)[1], this spontaneous electrical activity is assumed to have a major neurobiological function[2]. From theoretical considerations, the spontaneous spikes bursts are noise in the brain system, and as such it is important to determine their in-vivo statistical profile. From practical considerations, the spontaneous spikes burst are noise that is known to have many neurobiological effects, where too much or too little noise might have a negative neurobiological impact. For example autistics show high level of neuronal noise[9], while old adults have low neuronal noise compared to young adults (cognitive aging)[10]. However, until now the in-vivo statistical profile of the spontaneous firing of spikes has not been characterized. Here we suggest in-vivo methods to evaluate spontaneous firing rate in the brain and support our method from different perspectives.

To test our hypothesis and methods, we use: (i) mathematical analysis, (ii) simulations, (iii) in-vitro experiments on animal neuron networks data (iv) and in-vivo human fMRI and EEG data analysis. In particular we also tested our hypothesis, that during rest the neuronal noise is dominant, by introducing random noise into the Hopfield network model[11], by analyzing it mathematically. In recent years network modeling received ample attention, modeling of the networks between cells have been shown useful and is believed to progress further in future[12]. Moreover, recent advances in understanding complex networks, are attributed to modeling and simulations[13]. Nevertheless, spontaneous firing rate with its 1/f neuronal characteristics, has not been simulated yet.

Currently, the spontaneous background electrical activity have been analyzed via in-vitro works. In-vitro investigations of animal models introduced a range of estimations of the neuronal spontaneous firing rate, λ, depending on the neuronal cell type and on the animal model[2,14,15]. However, evaluating in-vivo mean firing rate λ of the resting brain by a direct invasive experimental wet lab measurements cannot be technically

[1]Department of Physics, Bar-Ilan University, Ramat Gan, Israel. [2]Research Institute of Science and Technology Innovation, Civil Aviation University of China, Tianjin, China. [3]School of Reliability and System Engineering, Beihang University, Beijing, China. [4]Hangzhou International Innovation Institute of Beihang University, Hangzhou, China. [5]These authors contributed equally: Hila Dvir, Shu Guo. ✉e-mail: dvirhil1@biu.ac.il; guoshu_1992@163.com

obtained, since the invasive measurement itself affects the mean firing rate, which is very sensitive to environmental changes. Moreover, in-vivo wet lab measurements of brain λ, cannot be categorized as rest state conditions, because the invasive measurement is physiologically stressful. In the present study we develop an in-vivo non invasive method to evaluate λ of the whole brain and of specific brain's functional systems during rest state based on non-inversive fMRI or EEG data.

Calculating the average value of the spontaneous firing rate for the ensemble of neurons within the whole brain is considered a challenging and difficult task, and even an harder task is to evaluate it in-vivo. This is since the neurons in the brain have vast interactions and links[16,17], and this characteristic is known to exhibit an extremely complex display[16–22]. Thus, the ensembles of neurons within the brain networks have different collective properties compared to a single neuron, e.g., different firing rate frequency behavior, and importantly, different spontaneous firing rate mean values[2]. Although the average in-vivo spontaneous firing rate of the brain is of foremost importance in neuroscience, e.g., for diagnostic and understanding of brain diseases, not much is known on its nature and on its value, which it is usually assumed to be below 0.1 Hz[1,23]. Here we develop an analytical framework to evaluate the average spontaneous firing rate for a given brain or for a functional system, using statistical signal processing analysis of the in-vivo blood oxygen level dependent (BOLD) based on rest-state fMRI signal.

We develop here a framework utilizing brain fMRI that could provide important insight on the brain's stochastic nature. Apparently, the BOLD signal of rest-state fMRI, shows spontaneous fluctuations in the low-frequency domain at wide range of frequencies below 0.1 Hz[1,23]. Therefore, it was generally accepted that the in vivo resting brain spontaneous firing rate is below 0.1 Hz. But, an important question is, which specific frequencies/frequency within this range are mainly responsible for this spontaneous fluctuations pattern seen in fMRI BOLD signal of individuals at rest[23]? Answering this question is important as it can provide a hint, as we show below, on the in-vivo average spontaneous firing rate of neurons at the rest-state for individuals.

The spontaneous oscillatory activity in the brain depends on both, the single neuron and the neurons network interactions properties[24]. It has been shown that the collective spontaneous activity of neuronal cultures elements in a network, have a power spectrum in the form of a power-law, even for different brain networks types. Specifically, the power spectrum of the neurons' network firing rate has a 1/f behavior at low frequencies <0.1 Hz[2,23]. This 1/f behavior is observed in neuronal cultures[2], fMRI signal, electroencephalography (EEG), magnetoencephalography (MEG) and even in human behavioral studies[23]. Although it is agreed that the 1/f behavior at low frequencies is not merely an artifact, its nature is not yet fully understood. It is even not known what frequencies range contributes to the 1/f behavior, e.g., does the ultra-low frequencies range also exhibit a 1/f distribution[23]?

In the present work, we develop a framework to answer the following questions (see ref. 23) concerning the 1/f low frequency behavior: What is the origin of the 1/f structure found in the power spectrum of neurons network assembly? what frequency values contribute to the 1/f behavior? How can we model and analyze the 1/f behavior at low frequencies? As we relate this 1/f phenomenon to the stochastic neuronal nature, we will address important issues regarding the nature and value of the in-vivo average spontaneous firing rate in the brain. We develop two different approaches, organized in three methods, to calculate the mean firing rate estimation during rest based on rest fMRI data. Our three methods apply to the two approaches: (i) Based on the BOLD signal spectrum, (ii) Based on temporal correlations of BOLD signals. In all our methods we obtain the mean firing rate estimation for each of the 710 participants in our database, and verify that indeed the three methods congruent. Another important support is obtained by comparing our indirect calculation of λ to a direct calculation of λ obtained from in-vitro experiments on animal neuron networks. For the fMRI and EEG in-vivo data, we also find that participants' mean firing rate estimation, λ, correlates with actual brain task performances, which indicates that our in-vivo λ evaluation will be useful for better understanding, evaluating, and monitoring brain functions and diseases.

Results

Basic hypotheses

Prior to presenting our suggested methods to calculate the in-vivo mean spontaneous firing rate, below we specify our basic hypotheses regarding the rest state and the autocorrelation.

The rest-state hypothesis

We wish to study here the effect of neuronal noise on the neuronal current spectrum and on its network connections. To this end we introduce random noise into the Hopfield network model[11]. This is based on our hypothesis that during rest, when there is no input to the network, the neuronal noise is dominant.

In the deterministic case, the Hopfield model describes basic concepts of the firing-rate and neuron membrane potential during stimulated activity[11,25] as,

$$\tau \cdot dV_i/dt = -V_i + \tau \cdot \sum_{j \neq i} W_{ij} R(V_j) + \tau \cdot I_{\text{aff}} \tag{1}$$

Here V_i is the membrane potential of the i-th neuron, τ is the integration time constant (equals to capacitance time resistance), $W_{i,j}$ is the strength of the synaptic connection between neuron i and neuron j, $R(V_j)$ is the firing rate of the j-th neuron, and I_{aff} is the afferent input.

In the present study we introduce the neuronal noise to the Hopdield model when there is no excitable afferent stimulation input to the system, as we assume to occur during rest. That is, instead of using deterministic I_{aff}, as used during stimulated activity, we assume for resting state the existence of random noise with zero mean as input I_{aff} and thus, we obtain,

$$\tau \cdot dV_i/dt = -V_i + \tau \cdot \sum_{j \neq i} W_{ij} R(V_j) + \tau \cdot \sigma \cdot n_i \tag{2}$$

where n_i is a standard white noise, which is assumed to have zero mean and σ is the standard-deviation. Assuming Eq. (2), means that the random noise input represents the rest state (hence the zero mean) in the environment of neuronal noise (having standard deviation σ). The mean of the firing rate is λ, so that:

$$\lambda = E\{R(V_j)\} \tag{3}$$

where $E\{\}$ is a mean operator.

Figure 1a shows R, as the inverse time gap between each two consecutive action potentials peaks, where the mean of all rates R defines λ. Such a random voltage, as in Eq. (2), which is affected by white noise, yields activation rate, R in Eq. (3), with inhomogeneous Poisson process statistics[26,27]. The inhomogeneous Poisson process has some resemblance with the homogeneous Poisson process, such as both counting probability with exponential λ decay, where λ is also the mean rate of the events[28]. In case of neurons, those events are the action potential bursts (above the threshold) events, i.e., the firing events, see Fig. 1a.

The autocorrelation hypothesis

We regard here to the autocorrelation of neuron's firing rate, r, as a mixture of inhomogeneous Poisson process and a small cosine fluctuations[29], as demonstrated in Fig. 1b:

$$r \equiv r(t_1 - t_2) = r(R(t_1), R(t_2)) = p \cdot \cos(2\pi f(t_1 - t_2)) + q \cdot e^{-\lambda \cdot (t_1 - t_2)}, \tag{4}$$

where $(t_1 - t_2)$ is the temporal gap between the two correlations. The term $q \cdot e^{-\lambda \cdot (t_1 - t_2)}$ represents the inhomogeneous Poisson process part, and the term $p \cdot cos(2\pi f(t_1 - t_2))$ represents the cosine fluctuations. The cosine fluctuations reflects findings that the firing rate of a neuron is modulated by

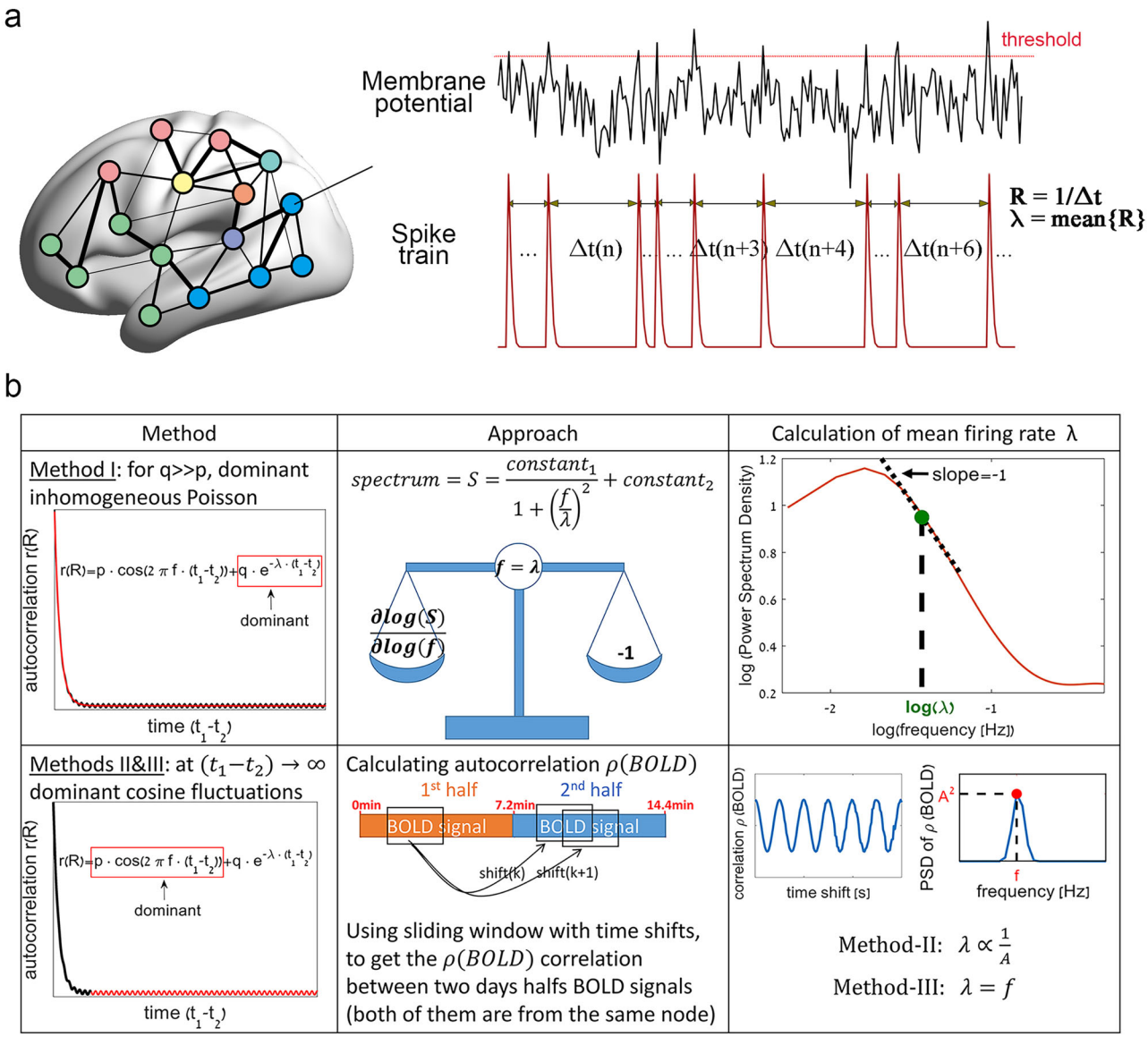

Fig. 1 | Illustration of our methods. a In our framework we hypothesize that at rest, there is no external input to the brain neurons and therefore the afferent input, I_{aff} in Eq. (1), is noise with zero mean, which we associate physiologically to the neuronal noise. Here we illustrate a simulated evolving voltage with this random noise input, I_{aff}, of zero mean. From time to time the obtained random voltage crosses the neuronal excitability threshold, and an action potential is formed. The inverse time gap between each two consecutive action potentials peaks defines the activation rate R, and the mean of all rates R defines λ. Such a random voltage, which is affected by white noise, yields activation rate, R, with inhomogeneous Poisson process statistics[2,6,27], which is used in our method-I. In our methods-II and III we use the physiological feature that R is also affected by a weak cosine fluctuation[29]. **b** In total, the autocorrelation of neuron's firing rate, r, is composed from dominant exponential (inhomogeneous Poisson process) and weak cosine expressions. Method I: Obtains λ from the fMRI BOLD signal spectrum (obtained from all neurons in brain's functional systems), and assumes that: (i) For the total autocorrelation the exponential expression is dominant (inhomogeneous Poisson process). (ii) The neurons are connected via extensive networking connections hence $constant_1 > > constant_2$. Methods II& III: Obtain λ from the fMRI BOLD signal autocorrelation (obtained from single node/voxel) between the two half's day, and assume that at temporal gap $(t_1 - t_2) \to \infty$ (relatively to λ) where the autocorrelation has cosine fluctuations.

a small and slow oscillation even in the absence of stimulation[30], and even under anesthesia[31]. Note that the cosine fluctuations of the neuronal current autocorrelation are very weak[29], and hence can be seen in specific conditions such as anesthesia, where disturbances are low. This is the reason why they are often been disregarded. Therefore, in Eq. (4), p and q are constants such that $p < < q$ (small cosine fluctuations), and f is a constant which describes the very slow oscillations[29].

In Eq. (4) (similar to ref. 29) the cosine fluctuations have a general frequency, f, however here we suggest that those fluctuations are not arbitrary but fluctuate with $f = \lambda$. This hypothesis is reasonable since λ has units of frequency ($[Hz]$, see Eq. (6) below), and since λ, like f, has very low values ($2\pi f$ describing very slow osculations[29]). We next test this hypothesis and support it.

Accordingly, Eq. (4) becomes:

$$r \equiv r(t_1 - t_2) = r\big(R(t_1), R(t_2)\big) = p \cdot \cos(2\pi\lambda(t_1 - t_2)) + q \cdot e^{-\lambda\cdot(t_1 - t_2)}. \quad (5)$$

Note that below we use Eq. (5) for method-III, while for method-I and method-II Eq. (4) is sufficient. That is, only for method-III we use our hypothesis that the cosine has a λ frequency.

Since the cosine fluctuations are very slow and since $p < < q$, the exponential autocorrelation, i.e, the inhomogeneous Poisson process, is dominant, such that the spectrum of the entire process is affected mostly by it. This inhomogeneous Poisson process is the base of our first approach: method-I demonstrated in Fig. 1.

In our second approach, we employ method-II & method-III as demonstrated in Fig. 1. Here, we use the fact that the small cosine fluctuations can be visualized when obtaining autocorrelations between two distinct temporal signals. This is since for two temporal signals, if the temporal gap is long, than the exponential part vanishes.

Therefore, our two approaches are based on two different types of neuronal processes, which describe two distinct phenomena: inhomogeneous Poisson process (which is dominant) and cosine fluctuations (which are small, seen only at long temporal gaps correlations). In this way, the value of λ for a given individual brain is validated by two independent approaches, and the results of excellent agreement between the methods, support also our three methods.

Suggested methods to calculate mean firing rate

We suggest here two different approaches, arranged in three methods, to calculate the in-vivo mean spontaneous firing rate in the brain, λ. All our three methods are also summarized in Fig. 1b.

First approach, method-I: mean firing rate estimation - based on the spectrum

The firing rate $R(V_j)$ is assumed to follow mostly an inhomogeneous Poisson process (see Eqs. (4) and (5) with $p << q$)[29], hence the spectrum of this autocorrelation, between two temporal values t_1 and t_2, decays as: $e^{-\lambda|t_2-t_1|}$[28] (see also our simulations in Supplementary Fig. S1i), which is unlike the homogeneous Poisson process. Assuming stationarity yielding that Eq. (2) at rest will show a current I spectrum (see Methods, Eqs. (13)–(16)) as follows:

$$S \approx \frac{c_1}{1+(f/\lambda)^2} + c_2 \tag{6}$$

where c_1 and c_2 are constants, such that $c_1 >> c_2$. Specifically, from the fMRI power spectrum analysis, we conclude that the c_2 value is less than 0.25 c_1 (see Supplementary Fig. S2). Moreover, note that from Eq. (16) below (see text immediately after Eq. (16)) we conclude that for brain neurons $c_1 >> c_2$, due to extensive networking connections and relatively low neuronal noise.

Analyzing Eq. (6) (see Methods, Eqs. (17)–(22)) yields,

$$\frac{d\log(S)}{d\log(f)} = -2 \cdot \frac{\left(\frac{f}{\lambda}\right)^2}{1+\left(\frac{f}{\lambda}\right)^2} \tag{7}$$

$$\left.\frac{d\log(S)}{d\log(f)}\right|_{f=\lambda} = -1. \tag{8}$$

Based on this analysis, using Eqs. (7) and (8) we can calculate λ of a given brain by identifying the point (shown as a green dot in Fig. 1b and in Supplementary Fig. S1a, d) where the slope of the power-low spectrum is -1. This is since at this point where $f \approx \lambda$ the slope $= -1$ (according to Eqs. (7) and (8)). In Supplementary Fig. S1g we show further support for this assumption, suggesting that particularly when the constants $c_1 >> c_2$ in Eq. (6), the point $f = \lambda$ on the spectrum is where the slope of the double-logarithmic plot of the power spectrum vs frequency is -1. In Supplementary Fig. S1h we specifically test method-I assumptions, by comparing between the mean firing rate λ as obtained from the model's simulated spikes train (x-axis) to method-I analysis (y-axis, as obtained using Eq. (8)). This comparison shows via simulations that the simulated firing rate corresponds well to the estimated firing rate of our method-I.

The BOLD signal measures neuronal ionic currents activity[32]. Hence next we implement our estimations on brain fMRI real data collected from 710 participants across two days, and find the neuronal mean firing rate estimation, λ, for each individual. Figure 1b (method-I) and Supplementary Fig. S2 show examples of fMRI BOLD signal spectrum demonstrating the point where the log-log plot slope is -1 (i.e., 1/f spectrum), which is the point where we expect $f = \lambda$ (Supplementary Fig. S3 show examples of EEG signal). Implementing this analysis on each of the 710 subjects we find a distribution of this λ as shown in Fig. 2a, indicating a clear peak at the most frequent value $\lambda \approx 0.045$ Hz, and an average value of $mean\{\lambda\} \approx 0.055$. Next, we test our hypothesize that our mean brain firing rate estimation is typical for a person and is not expected to change much in different days. To this end, we compare in Fig. 2b the fitting of our λ estimations between day-1 to day-2 of the fMRI measurements. Indeed, we find a good agreement with correlation of ≈ 0.60 between the estimated mean brain firing rate at the different days, thus supporting our hypothesis. In Fig. 2c we extend this analysis to calculate λ from 16 segments within each subject, obtaining correlations of $\approx 0.46 \pm 0.14$ for the same subject. Similarly, we also calculate the correlation of λ between different subjects (randomly selected), revealing a much lower correlation values ($\approx 0.02 \pm 0.10$) compared to those of the same person.

For 29 participants we performed a follow-up of measuring λ again after one to 11 months (re-test) from the original measurement (test), those results are shown Fig. 2d which illustrate a good and significant correlation of 0.62 (p-val = 0.0003) between the test and the re-test. This correlation of 0.62 resembles the 0.58 correlation seen in Fig. 2b for different days, where we expect λ to be consistent (though could show some degree of alterations) for a specific person at the re-test.

To further test our framework for evaluating the mean value of firing rate λ, per person, and support our hypothesis on the role of neuronal afferent current noise during rest, we next compare our estimated λ using an independent approach developed below. All methods are summarized and demonstrated in Fig. 1.

Second approach, methods-II & III: mean firing rate estimation - based on long term autocorrelation

Here we develop two further methods to evaluate λ based on a very different perspective than method-I. While in method-I we used the inhomogeneous Poisson description, which is the dominant characteristic of the neurons' firing rate at short time scales, in methods-II & III we focus on the small cosine fluctuations that can be seen only at long-term scalings, $(t_1 - t_2) \to \infty$ relatively to λ. Since the two approaches, of method-I vs. methods-II & III, are independent and distinct in their perspectives, obtaining similar values of λ for the same subject will support our approaches.

For our calculations we use correlations between two temporal BOLD signals, so that the inhomogeneous Poisson process part in Eq. (5) vanishes, that is, $e^{-\lambda\cdot(t_1-t_2)} \to 0$. Hence, in our data we split the BOLD signal into two halfs: 1st half ($half_1$) and 2nd half ($half_2$), expecting that there is only a short neglectable tail (of less than 5% of the total samples), so that the inhomogeneous Poisson process part vanishes, remaining mainly with the cosine fluctuations part.

Using statistical signal processing tools, we find that the BOLD signal correlation ($\rho(BOLD)$) between the two halfs ($half_1$ and $half_2$) and the firing rate correlation (R), have the following relation (see Methods, Eqs. (23)–(39)):

$$\rho(BOLD_i^{half_1}, BOLD_i^{half_2}) = \frac{cov\left\{R_i^{half_1}, R_i^{half_2}\right\}}{\lambda}. \tag{9}$$

where i represents neuron i.

Since from Eq. (5) we get that at $\lambda \cdot (t_1 - t_2) \to \infty$ (two different halfs):

$$cov\left\{R_i(V)^{half_1}, R_i(V)^{half_2}\right\} = p \cdot (\cos(2 \cdot \pi \cdot \lambda \cdot t)), \tag{10}$$

it follows,

$$\rho(BOLD_i^{half_1}, BOLD_i^{half_2}) = \frac{p \cdot (\cos(2 \cdot \pi \cdot \lambda \cdot t))}{\lambda}. \tag{11}$$

Thus, from Eq. (11) we conclude that $\rho_i(BOLD) \equiv \rho(BOLD_i^{half_1}, BOLD_i^{half_2})$ fluctuates with amplitude proportional to $(1/\lambda)$,

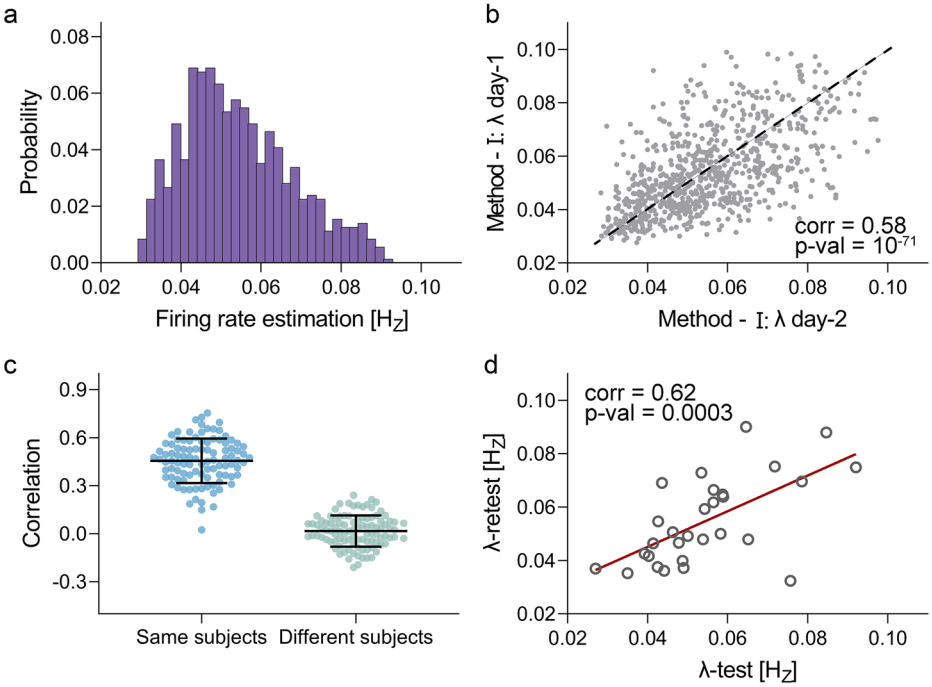

Fig. 2 | Mean firing rate estimation λ, as obtained from method-I, for each of the 710 participants fMRI records. a Distribution of λ across the tested population shows that the most probable λ is close to $\lambda \approx 0.045$, and mean of $mean\{\lambda\} \approx 0.055$. **b** Scatter plot of λ of two days for each participant shows correlation of $corr = 0.58$ (best fit is the dashed black line). Note that the estimation of λ is affected by measurement noise, hence might be improved if the BOLD signal could be calculated from fMRI data collected in several days. Since here the data is obtained from two days, in (**a**) and in the following analyses we use averaged λ of two days. **c** Correlations distribution of λ among subjects as calculated from dividing the temporal data to 16 segments each of time span 3.6 min. The analysis show correlation values $\approx 0.46 \pm 0.14$ within same subject, and correlation of $\approx 0.02 \pm 0.10$ for different subjects randomly selected. This analysis clearly strengthen the support of panel (**b**) i.e., the validity of our method-I. **d** For 29 participants we calculated λ again after several months (re-test after one to 11 months) from the original calculation (test), and obtain significant correlation of 0.62 between the two measurements. As it is expected that λ has consistent value for individuals (though could have some level of alterations) at the re-test, this result strengthen our calculation. Note that, panel (**b**) includes $N = 767$ subjects, and in order to avoid measurements errors in (**a**) and in following analyses we only consider people with λ values differences between the two days below 40%. Therefore, the data in (**a**), in (**c**), in (**d**) and in all following analyses include only $N = 710$ subjects (out of the total $N = 767$). Note, that out of the total 994 participants we include $N = 767$, since we removed participants with extrema head motions or participants for which λ could not be measured. Several examples of individuals PSD and their λ can be found in Supplementary Fig. S2.

and frequency $f = \lambda$. Hence, in method-II we analyze the two halfs correlation ($\rho(BOLD)$) amplitude, A, and in method-III we analyze its frequency, f. Note that while in method-III we use our hypothesis that the cosine has a frequency $f = \lambda$ (i.e., using Eq. (5)), in method-II we do not use this hypothesis and explore only the amplitude (i.e., just Eq. (4), along with Eq. (9)).

In Fig. 3a we demonstrate a typical example of the two half's day autocorrelation (same participant, same node, one window sliding with time shifts), representing $\rho(BOLD_i^{\text{half}_1}, BOLD_i^{\text{half}_2})$. This figure shows clear fluctuations around zero. In Fig. 3b the amplitude and frequency of those fluctuations are calculated as $A = \sqrt{1.70}$ and $f = 0.057$ (the x-y values of the maximal peak). This peak represents the cosine fluctuations value in the noisy environment. Note that, as expected from mean spontaneous firing rate, i.e., the value of this peak frequency, f, is lower than 0.1 Hz. Moreover, adding white noise to the original BOLD signal, in Fig. 3c–d, eliminate the cosine fluctuations of the auto-correlation, which strengthen our approach.

Since we hypothesize that f and $1/A$ are related to λ, we wish next to compare their values and trends within the different individuals. Indeed, Fig. 4a–c shows a significant high similarities represented by high Pearson correlations between the three methods, of $corr = 0.86$ (panel a), $corr = 0.69$ (panel b) and $corr = 0.88$ (panel c), all with $p\text{-val} < 10^{-101}$.

The highest correlation is $corr = 0.88$ between method-II, $1/A$, and method-III, f, (panel c), is not surprising considering both methods are derived from the same approach (the small cosine fluctuations). Nevertheless, it highly supports $f = \lambda$, i.e., that the frequency of the cosine fluctuations indeed relates to λ, as we hypothesize in the transition from Eqs. (4) to (5). This is a strong support for Eq. (5) since in method-II we do not use method-III hypothesis that $f = \lambda$ (for method-III we use Eq. (5), for method-II we use just Eq. (4)).

The next high correlation, with value of $corr = 0.86$, is between method-I and method-II described in Fig. 4a. This high correlation supports highly both, method-I and method-II, as they derive from very distinct approaches.

Comparing method-I and method-III in Fig. 4b also show high correlation of $corr = 0.69$, which together with the results of Fig. 4a strengthen our two distinct approaches. Note that in Fig. 4b, the values range of λ and f are similar, as expected. Moreover, comparing the histograms of λ to the histogram of f in Fig. 4d, show close relation between the firing rate values of method-I (from first approach) and method-III (from second approach). The small differences in the values of method-I and method-III can be related to the differences in the way method-I and method-III calculate the averaged values for each participant. Specifically, in method-I we calculate λ from an averaged spectrum (averaged PSD from all voxels, see Methods and Supplementary Fig. S2), whereas in method-III and method-II we calculate f and A from each voxel's correlation after which we average the obtained f and A values.

In Fig. 4e we compare correlations between different time frames: (i) original measurement and (ii) measurement performed 1-11 months later (retest); all this between our three methods: λ, f and $1/A$. The high correlations, between our methods, seen even after several months (retest) adds an important support to our suggested methods. Note that it is expected that after more than a month later, mean spontaneous firing rate could alter to some degree, as a result of environmental changes. Therefore, we see in Fig. 4e higher correlations when comparing methods within the same time frames, and lower, but still high correlations, than when comparing methods after 1-11 months later.

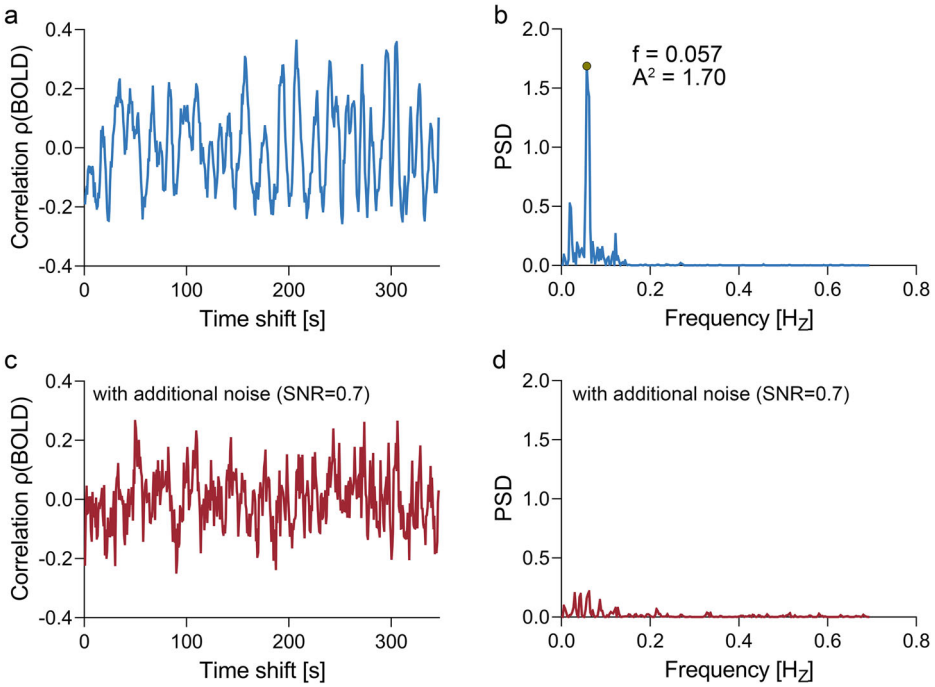

Fig. 3 | Demonstration of the evaluation of λ using method-II via A, and method-III via f. **a** Real fMRI data example of the two half's day correlation $\rho(BOLD)$ of a given subject. **b** Power spectral density (PSD) of the signal in the panel (**a**). To calculate the mean firing rate estimation using methods-II & III, we use the amplitude A and the frequency f of the maximal peak values (marked in a full gray circle). This example applies to a single voxel same person during rest-state. In order to calculate and obtain a single value for each subject, we average the values of f and A^2 from all nodes (i.e., $1/\sqrt{mean\{A^2\}}$ for method-II, and $mean\{f\}$ for method-III). In panels (**c**, **d**) we added white noise with $SNR = 0.7$ to the original BOLD signal and performed same analysis as in panels (**a**, **b**). Comparing the results of panels (**a**, **b**) to the results of panels (**c**, **d**) show noisier correlation (panel **c**) with much less dominant peak in the PSD analysis (panel **d**). This strengthen our conclusion on the importance of calculating f and A using the autocorrelation.

In conclusion, the results in Fig. 4a–e highly suggest that our two distinct approaches (three methods) to estimate mean firing rate are congruent. Considering Eq. (11), a future work could include also estimation of individual's p (the constant p is defined in Eq. (5) and in ref. 29), to further improve the correlations between the three developed methods.

Mean firing rate estimation of different functional systems

Having calculated the in-vivo mean firing rate estimation, λ, for the whole brain, it is interesting to find out what are the values of λ for the different brain's functional systems. First we test if we can implement our three methods (as shown in Fig. 1b) to each functional system separately. For this purpose, we show in Table 1 the fitting for all subjects when comparing between mean firing rate estimation of the three methods, for six brain functional systems. Specifically, this analysis is similar to Fig. 4a–c, but instead of considering the whole brain tissue, the analysis in Table 1 applies separately to six different functional systems. The good fitting, expressed by a Pearson correlation between $0.63 < r < 0.91$, supports the conclusion that our three methods are indeed suitable also for evaluating λ within each system separately.

Next, we investigate the distribution of λ across brain functional systems. Figure 5a analyzes the mean firing rate estimation of the each participant, as obtained from method-I, for the different functional systems, showing similar values for the different areas, all around $mean\{\lambda\} \approx 0.055$. Since different functional systems are interacting[16,33], linked and synchronized[17,21,34,35] to great extent for enabling the performances of complex tasks, we thus expect λ of different functional systems to have similar values.

From the same physiologically reasoning, it is expected that a subject with a relatively high value of λ in one functional systems, will also have relatively high values of λ in all other functional systems. That is, although λ of all brain systems are similar, the λ of different functional systems of the same subject correlate in their specific values. Indeed, Fig. 5b shows significant correlations (of 0.69–0.93, all with p-val <0.05) between the λ's of different functional systems in the same brain for different people (see also Supplementary Fig. S4). Our finding (Fig. 5b) that λ of the different functional systems in the same subject are indeed synchronized, as conjectured, adds an important support to our hypotheses and methods developed here.

In Fig. 5c we show the frequency f, that estimates mean firing rate using method-III, across the brain map after averaging f over all 710 participants. Using method-III, the firing rate can be evaluated for all functional systems, including the Limbic system. This is unlike method-I (Fig. 5a, b) which cannot be applied to analyze the Limbic system. Note that Fig. 5c suggests that the Limbic system contains the highest values of mean spontaneous firing rates, compared to the other functional systems. Moreover, interestingly, all brain functional systems in Fig. 5c show large similarity between f values of left (L) and right (R) hemispheres, which indicates a significant symmetry or synchronization between mean spontaneous firing rate of left and right brain hemispheres.

Calculating λ for in-vitro neurons' networks

Reproducing our computational method to calculate λ for in-vitro neurons' networks is an important and alternative step for validation of our approaches, particularly since such in-vitro experimental work could also provide direct measurements of the actual λ, and due to its closeness to the model of neuronal network. To this end, we analyzed recordings of spontaneous firing rate spikes from: (i) isolated leech ganglia for recording of motoneurons network[2], and (ii) hippocampal cultures from Wistar rats which were plated on multielectrode array[2]. From those recordings of the electrophysiological activity, λ is obtained directly by averaging the firing rate of the spontanious spikes. This could be compared, for validation purposes, to our method-I of calculating λ using power spectrum density (PSD) analysis as shown in Fig. 1b.

Therefore, in Fig. 6 we calculate λ using our method-I, from the PSD, for intact leech ganglia (Fig. 6a) and dissociated cultures of rat hippocampal neurons (Fig. 6b), and compared it to the direct measurements of λ (Fig. 6e and f, respectively). These results show indeed close values when comparing λ from our method-I vs. the direct experimental result, for both leech and rat hippocampal networks. Specifically, this comparison shows, accordingly, $\lambda = 0.18$ Hz (our method-I) vs. $\lambda = 0.21$ Hz (direct) for leech network, and $\lambda = 0.31$ Hz (our method-I) vs. $\lambda = 0.34$ Hz (direct) for rat hippocampal network. Note that those values are related to mean spontaneous firing rate per-neuron, after dividing the mean firing rate by the total number of neurons in the culture (see Supplementary). Interestingly, those values of animal in-vitro neuronal cultures λ are higher than the human fMRI in-vivo λ.

Thus, Fig. 6 supports via in-vitro experimental records our method of calculating λ for two very different networks. Not only that the networks origins are different (leech and rat), but even the network connections are distinct: intact ganglia and dissociated cultures. Therefore, unrelated to the networking type and value, we obtained support to our method. Note that,

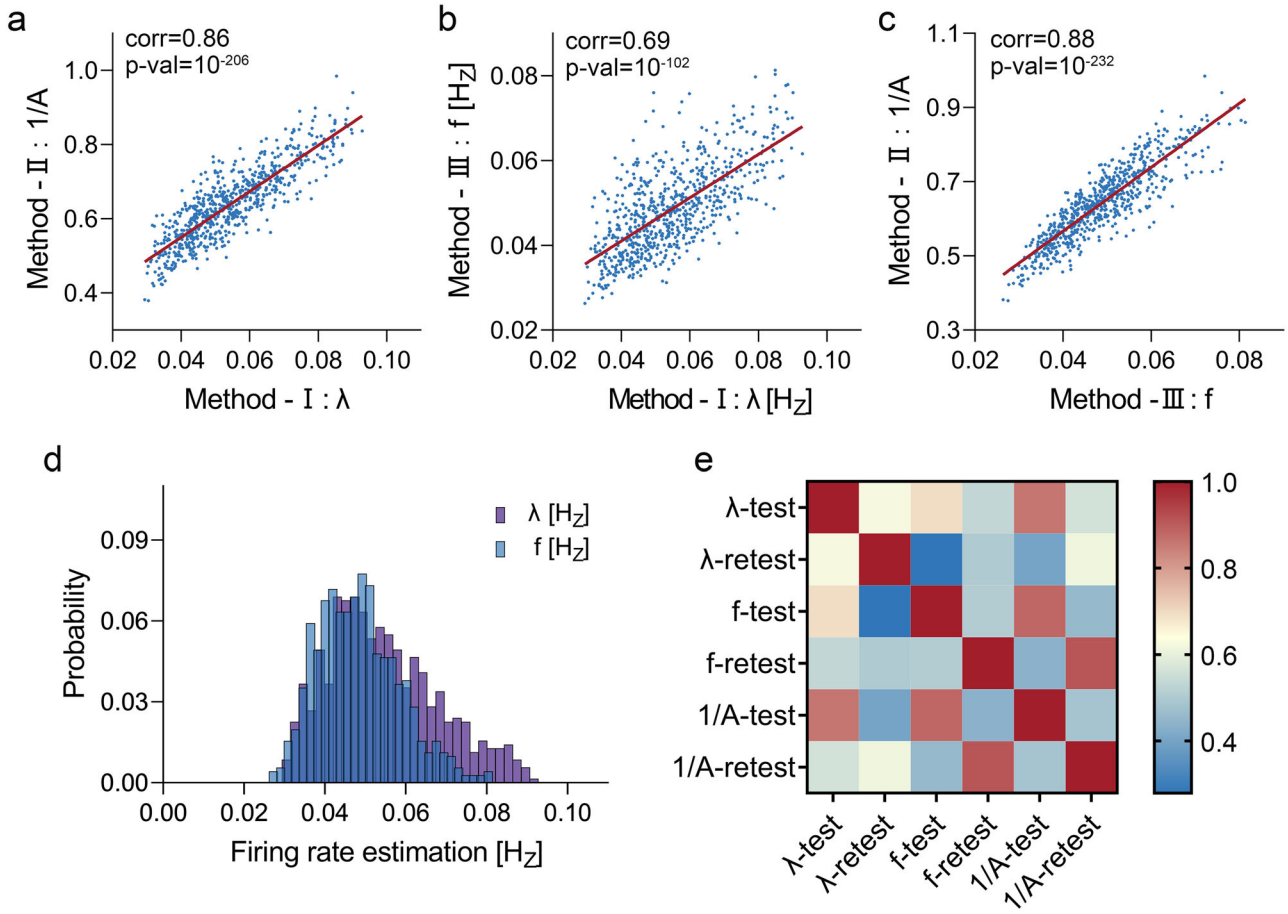

Fig. 4 | Comparing our three developed methods to evaluate the mean firing rate of an individual. a Comparing for different subjects λ as obtained from BOLD fMRI signal spectrum (method-I), to the correlation $\rho(BOLD)$ amplitude A (method-II). **b** Comparing λ for different people as obtained from our suggested method-I, to the correlation $\rho(BOLD)$ frequency f (method-III). **c** Comparing A as in our suggested method-II, to the correlation frequency f as in our suggested method-III. All comparisons in panels (**a**–**c**) show excellent correlations (all with p-val $<10^{-101}$) of **a** $corr = 0.86$, **b** $corr = 0.69$ and **c** $corr = 0.88$. **d** Histogram analysis show close relations between the values of method-III f (blue) and of method-I λ (purple) for different people. The close similarity between the histograms of the two methods represents an additional support for our methods. Note that an important technical difference between method-I and method-III, is that in method-I we calculate λ from a spectrum averaged across voxels (see Methods and Supplementary Fig. S2), while in method-III (and in method-II) we calculate f (and A) from each voxel's correlation PSD. Therefore, we expect some differences when comparing method-I results to those obtained by the second approach, f and A, in estimating mean firing rate. **e** Correlations between our three methods at same time frame (test) and after one to 11 months (re-test).

interestingly, the in-vitro PSD and its derivation (both for leech network in Fig. 6a, c and for rat hippocampal network in Fig. 6b, d), show resemblance to the in-vivo fMRI PSD and its derivation (Supplementary Fig. S1a, d).

Relation between individuals λ and brain task performances

A major challenge in brain research is to relate measured brain parameters to actual task performances. As we offer here a method for in-vivo λ evaluation, it is of much interest to test whether the mean spontaneous firing rate, λ, could be related to task performances. Therefore in Fig. 7a we present the correlation values between the λ value of a subject and three types of task performances: motor (Fig. 7a, blue), working memory (Fig. 7a, green and red), and attention (Fig. 7c). Additionally, Fig. 8a use EEG data[36] to calculate λ values (using our method-I) pre- vs. post-tasks with cognitive trainings, such as working memory tasks. Since also EEG data known to show a 1/f behavior[23], we expect that our method-I can be applied also to EEG data, and hence can observe changes of λ after cognitive tasks. Since the tasks are performed in short duration, we expect small but significant differences in λ.

As λ reflects both excitability threshold and neuronal noise, we suggest that some tasks correlates with λ due to its neuronal noise characteristic, and some due to its excitability threshold characteristic (the specific tasks 1–18 are described in Supplementary Fig. S5):

Table 1 | Correlations of mean firing rate estimations between our three methods, for different brain functional systems and different people

functional system	method-I vs. method-II	method-I vs. method-III	method-II vs. method-III
visual	0.84*	0.77*	0.87*
somatomotor	0.83*	0.71*	0.82*
dorsal attention	0.77*	0.80*	0.82*
ventral attention	0.77*	0.63*	0.84*
frontoparietal	0.72*	0.76*	0.80*
default mode	0.77*	0.76*	0.91*

This table is in accordance to Fig. 4 panels (a)-(c). All results are statistically significant with $^{*}p$-value $< 10^{-50}$.

An example for a neuronal noise characteristic affecting both task performances and λ is the motor grip strength test, shown in Fig. 7a (blue) and Supplementary Fig. S6a. Noise in the action potential aimed towards the muscle fibers, contributes to force variability, which in turn reduces the twitch strength in the innervated muscle fibers[37]. Therefore high neuronal noise, which is known to increase λ, is expected to also decrease the motor grip strength. In Fig. 7a it is indeed found that there is a negative correlation

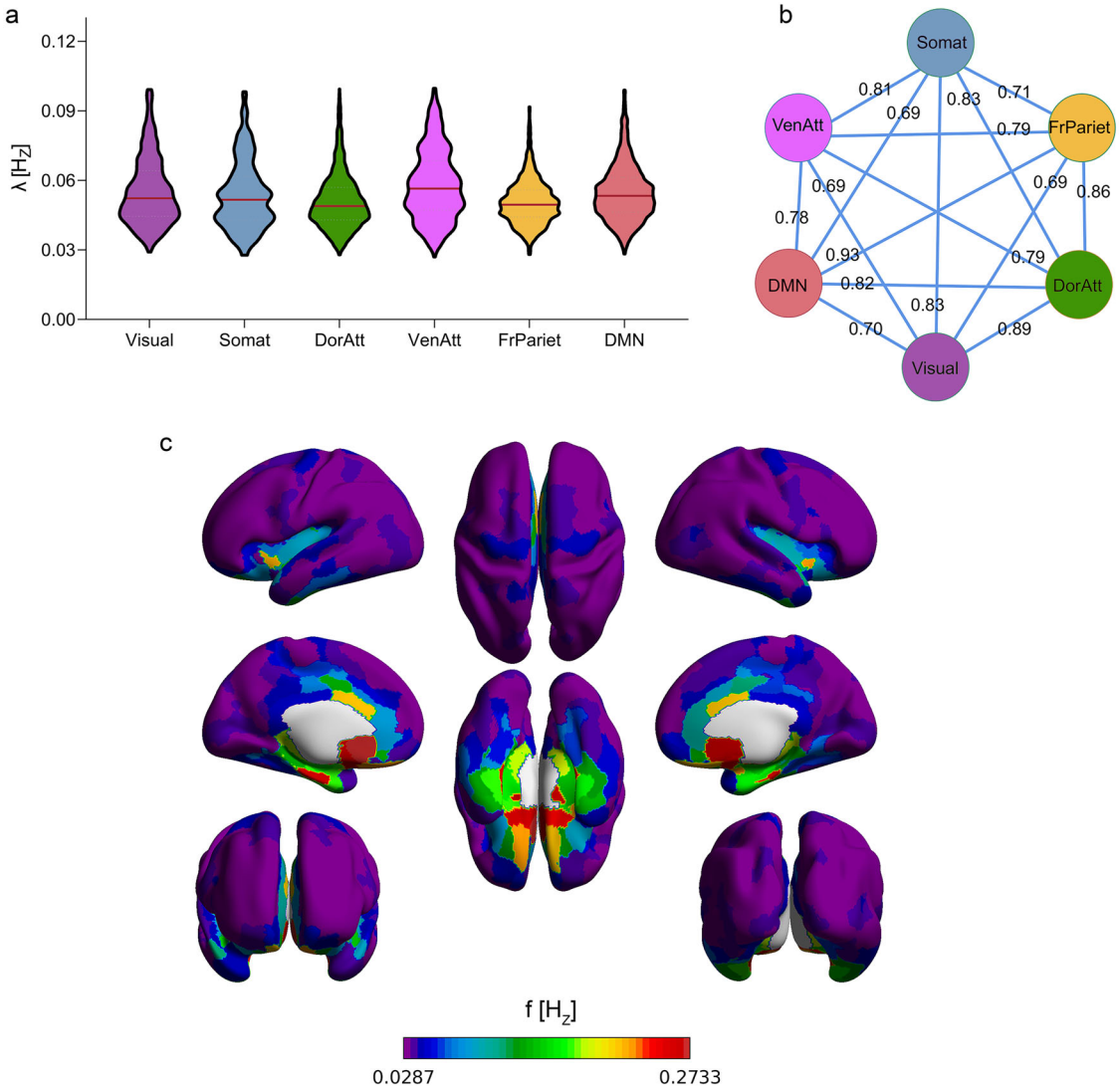

Fig. 5 | Functional systems analysis. Evaluating λ based on **a**, **b** method-I and **c** method-III. **a**, **b** Analysis of the average firing rate, λ, for all participants for each of the different functional systems: Visual, Somatomotor, Dorsal Attention, Ventral Attention, Frontoparietal and Default Mode. This includes all functional systems except the Limbic, for which we find that the condition $c_1 >> c_2$ in Eq. (6) is not valid, and consequently does not show a slope of -1 on its spectrum. **a** The λ value spreading along population of $N = 710$ participants for the different functional systems. The mean value of λ is close to 0.055 for all functional systems, without statistical significant differences. **b** Analyzing the compatibility of λ between different functional systems within the same participant, shows that the values of λ are highly correlated (correlations between 0.69 and 0.93, all with P-val < 0.05). **c** Frequency brain map, f, in order to estimate the mean firing rate using method-III. The shown frequencies f are averaged values for all 710 participants. Note that in panel (**c**) the Limbic system is included. While, due to high neuronal noise, method-I cannot be used to estimate Limbic system, method-III (and method-II) can evaluate the Limbic average firing rate.

between motor strength task and λ, as expected. In Fig. 7b, we show a strong negative correlation between method-III frequency, f, and the motor strength task. Since λ and f are correlated, Fig. 7b suggests that f and motor strength task also have strong negative correlations. Interestingly, the correlations with f have non-symmetric values when comparing left and right hemisphere.

An example for an excitability threshold characteristic affecting both task performances and λ is the relation between λ and the accuracy of working-memory (WM), shown in Fig. 7a (red) and Supplementary Fig. S6b. Neuronal excitability is associated with WM performances, as was found in previous works studying WM from genetic[38], dopamine modulation[39] and neuronal modeling[7] perspectives. Interestingly, we find in Fig. 7a that WM performances are positively correlated with λ, where participants with better WM performances (higher accuracy and reduced reaction time) have higher values of λ and hence lower excitability threshold (i.e., higher excitability).

An example for task performance effected by both excitability threshold and neuronal noise (as is the case for mean firing rate) is the attention (see Fig. 7c). Attention is effected by both excitability threshold[40] and noise[41], whereas higher attention is obtained with higher threshold and lower noise, therefore attention and mean firing rate are effected oppositely. This in agreement with Fig. 7c, which shows negative correlation between mean firing rate estimation, measured according to method-III f, and the task performance related to attention: Short Penn Continuous Performance Test (SCPT) Sensitivity. Interestingly, Fig. 7c, which marks only significant correlations, indicates that this brain area which show significant correlations between SCPT and mean firing rate estimation, uniquely relates to left-Inferior-Parietal. Importantly, this specific brain area of the left-Inferior-Parietal has been found to have a role in attention[42].

We note that there are also other behavioral characteristics, in additional to motor, WM and attention, which show strong correlation with mean firing rate, and which could be analyzed and discussed in future studies.

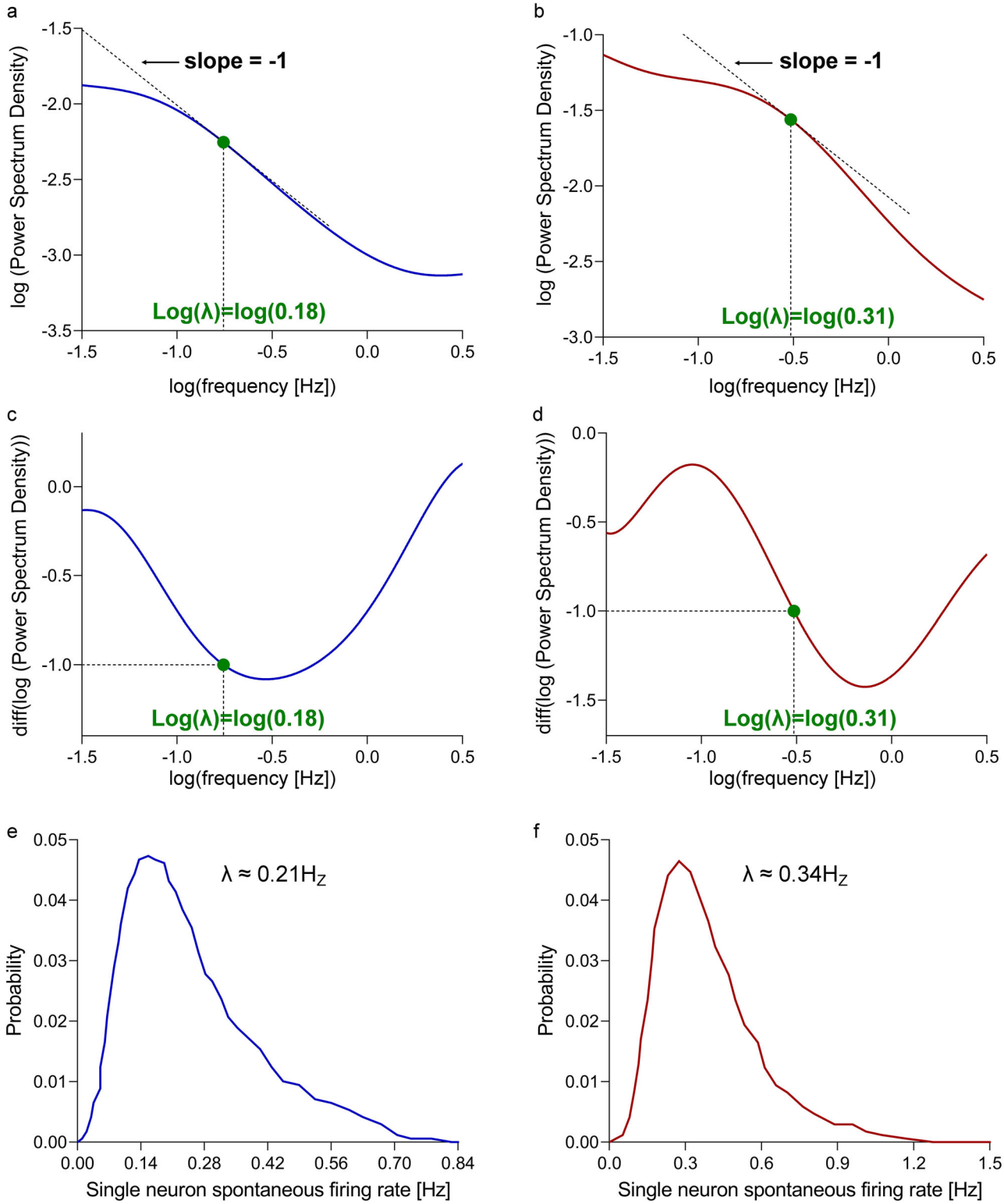

Next we show not only that our method-I is valid also to EEG data, but also that the λ from EEG changes when measured after cognitive tests. Technically, the EEG record voltage potentials resulting from summation of currents flow in and around neurons, which then conduct throughout the brain volume to the EEG electrodes[43]. Due to noise, unlike the fMRI, from the EEG data the spectrum of low frequencies (bellow 0.1 Hz) cannot be obtained. However, it has been suggested how to overcome this issue by subtracting the envelope of alpha wave[23,44]. Here we use this technique to obtain PSD of low frequencies EEG, followed by measuring λ using our method-I. Note the similarity of PSD when comparing the fMRI PSD in Supplementary Fig. S2 and the EEG PSD in Supplementary Fig. S3, to the theoretical (analytical equation) PSD in Supplementary Fig. S1b.

In Fig. 8a, blue line, we show the distribution value of λ for 585 subjects, with mean value of $\lambda_{EEG} \approx 0.134$ Hz for data collected pre-tasks. Since the EEG alpha waves are attributed to the activity of cells in the Thalamus[45], and since the Thalamus is anatomically close to the Limbic system and has close

Fig. 6 | Analysis of the in-vitro spontaneous activity of two neuronal cultures networks. a, **c**, **e** Leech ganglia (in blue lines) and **b**, **d**, **f** rat hippocampal neurons (in red lines). Power-spectrum density (PSD) of the neurons network firing rate as measured in-vitro from **a** intact leech ganglia and **b** dissociated cultures of rat hippocampal neurons[2]. Both PSD (of leech and of rat) are obtained after smoothening with truncate median filter of 50 order, followed by a polynomial fit (9 order polynomial fit). The green dot represents the polynomial value where its derivative is −1, and the doted black line represent the −1 slope around this dot. Measuring the frequency where the PDS slope is −1 (see Fig. 1a), our method-I analysis of this experimental data suggest that a single neuron spontaneous firing rate is **a** of $\lambda = 0.18$ Hz for leech ganglia, and **b** of $\lambda = 0.31$ Hz for rat hippocampal neurons. The PSD derivatives of (**a**, **b**) are shown in (**c**, **d**), which also show, in green dot, the first frequency where the slope is −1. As before, for method-I, we take λ as the first solution where the polynomial obtains −1 slope (within the PDS frequencies range). The values of λ, as calculated in pannels (**a**, **b**) and in (**c**, **d**), are supported in panels (**e**, **f**) where spontaneous spikes frequency distribution of the firing rate in (**e**) leech and (**f**) hippocampal neurons were measured directly[2], obtaining mean values of (**e**) $\lambda \approx 0.21$ Hz for leech and (**f**) $\lambda \approx 0.34$ Hz for hippocampal neurons' networks. Note that, for panels (**e**) and (**f**), in order to find the single neuron spontaneous firing rate, we used the network firing rate (defined as the sum of all neuron firing rates[2]) and divide it by the total number of neurons in the network (see last section in Supplementary).

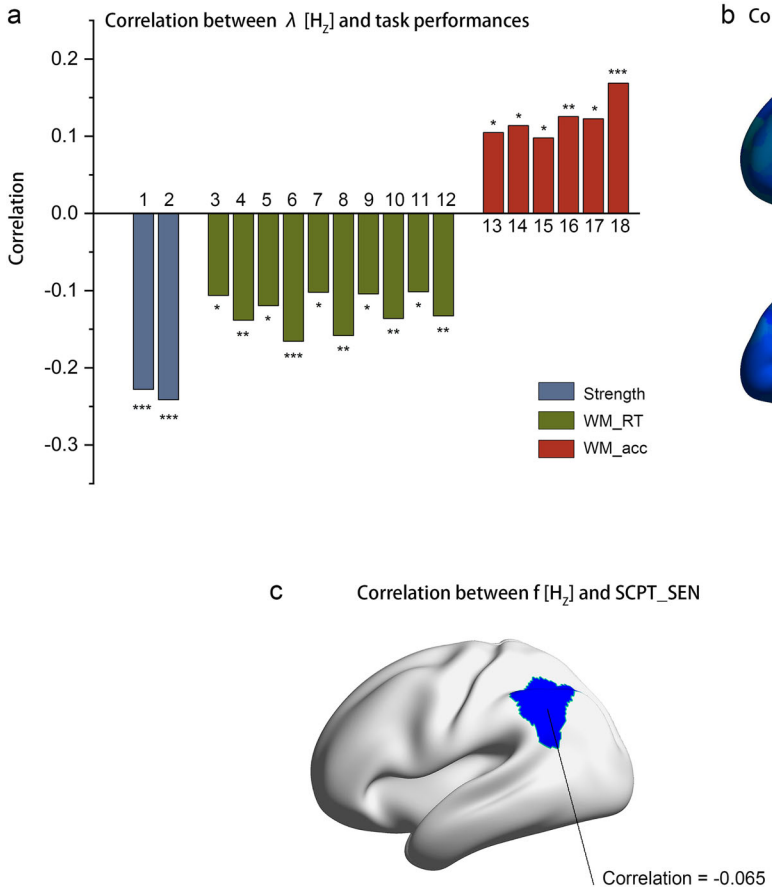

Fig. 7 | Behavioral measures and their correlation with our measured mean spontaneous firing rate. a Correlations between λ, calculated from the whole brain, and behavioral measurements of motor (blue) and working memory (green and red). The motor is shown for motor grip strength, and the working memory (WM) is demonstrated for task accuracy (in red) and reaction time (RT) (in green). All shown correlations are significant, with $^{*}p$-value <0.05, $^{**}p$-value <0.01 and $^{***}p$-value <0.001. The specific tasks 1–18 are described in Supplementary Fig. S5 in the supplementary. Detailed correlations, between λ and additional motor and WM behavioral measurements, are shown in Supplementary Fig. S6. **b** Correlations brain map between mean firing rate estimation, measured according to method-III *f*, and motor grip strength task performance. Note that a detailed correlation, for each brain's functional systems and for each specific task, can be found in Supplementary Fig. S6. **c** Correlations brain map between mean firing rate estimation, measured according to method-III *f*, and the attention task performance, measured by Short Penn Continuous Performance Test (SCPT) Sensitivity. Only significant (p-val <0.05) correlations are shown. Note that the unique brain region that correlates with SCPT-Sensitivity is left-Inferior-Parietal, which has been reported related with attention[42], whereas all other brain areas, including right-Inferior-Parietal, are not significantly correlated.

functional relationship with it[46], it is not surprising that we find EEG λ values to be close to the fMRI λ value of the Limbic system (see fMRI Limbic system $\lambda \rightarrow 0.15$ Hz in Fig. 5c). Note that the λ of the Thalamus, which is a deep brain structure, cannot be obtained using fMRI data, which can measure only surface brain structures, hence the EEG is complementary to the fMRI in this sense.

Importantly, comparing mean values of λ pre-tasks (blue) to post-tasks (red), from Fig. 8a, shows that the λ values are consistently lower after tasks. While mean value of $\lambda_{EEG} \approx 0.134 \pm 3.8 \cdot 10^{-4}$ [Hz] for data analyzed pre-tasks, the mean value of $\lambda_{EEG} \approx 0.131 \pm 4.5 \cdot 10^{-4}$ [Hz] for post-tasks. Though the difference in λ is small, it is highly significant showing two-sample t-test p-val $= 1.1 \cdot 10^{-6}$ and two-way ANOVA (analysis of variance) p-val = 0.002. This conclusion can be observed also directly from Fig. 8a histograms, where λ pre-tasks histogram (blue line) is compared to λ post-tasks histogram (red line), showing higher probability of the λ post-tasks histogram to occupy lower values of λ. We hypothesize that for longer period of tasks the difference in λ might further increase. Note that the tasks includes cognitive tasks of: selective attention and executive functions tasks[36]. This trend, where λ is decreasing after cognitive tasks, which contain attention tasks[36], matches our finding in Fig. 7c that show negative correlation between fMRI mean firing rate estimation and attention.

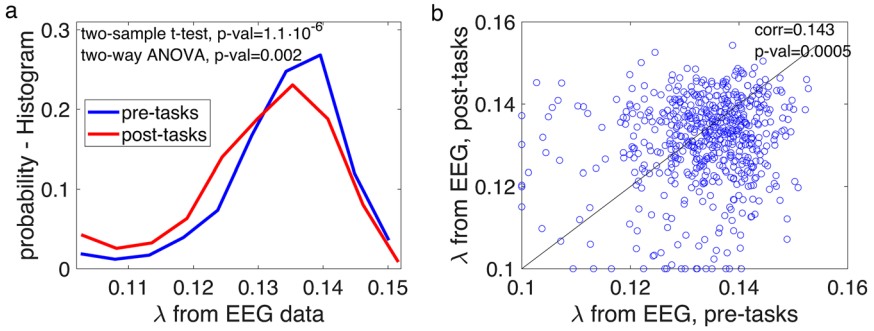

Fig. 8 | The values of λ obtained from the EEG data at the resting state. The EEG data[36] have been used to obtain λ based on method-I, in a similar way as for the fMRI data. The EEG data include pre-tasks and pot-tasks analyses of 585 participants obtained during rest with eye closed. Due to noise, in accordance with the literature[23,44], we use only EEG signals that relate to alpha wave, which is known to be attributed to the activity of the Thalamus[45]. As the Thalamus is anatomically and functionally close to the Limbic system[46], we indeed find EEG λ values close to the fMRI λ value of the Limbic system (see Fig. 5c). **a** λ values distributions for 585 participants pre-tasks (blue) and post-tasks (red) from EEG data as obtained from method-I. Note that post-tasks values tend to occupy lower values of λ when compared to pre-tasks λ values. This conclusion is further strengthen when looking at the averaged values. Average values analysis shows pre-tasks with mean value of $E\{\lambda\} \approx 0.134 \pm 3.8{\cdot}10^{-4}$ [Hz] is higher then the post-tasks with mean value of $E\{\lambda\} \approx 0.131 \pm 4.5{\cdot}10^{-4}$ [Hz]. The 585 subjects show significant difference between λ pre-training vs. λ post-training, with two-sample t-test with p-val = $1.1{\cdot}10^{-6}$, and two-way ANOVA (analysis of variance) p-val = 0.002. This points on a small but significant decrease of λ after tasks. **b** We find the matching between λ pre-tasks and λ post-tasks, with statistically significant correlation of 0.143 and p-val of 0.0005. A significant (p-val = 0.0005) correlation of 0.143, point on a tendency of the λ post-tasks and the λ pre-tasks to have the same trend, where there are other factors effecting post-tasks performances in addition to the pre-tasks λ.

Moreover, it is expected that there will be some relationship between λ pre-tasks vs. λ post-tasks, that is participants with high λ pre-tasks will show high λ post-tasks, and vise-versa. Hence, in Fig. 8b we compared the λ pre-tasks to the λ post-tasks, which show significant correlation of 0.143 with p-val = 0.0005, for 585 participants. Note that the a significant (p-val = 0.0005) correlation of 0.143, point on a tendency of the λ post-tasks and the λ pre-tasks to have the same trend, where there are other factors effecting post-tasks performances in addition to the pre-tasks λ.

Discussion

In the present study we use stochastic analysis aimed to answer fundamental questions in neurology. By analyzing the nature of 1/f fluctuations at rest state fMRI (and EEG), we propose to answer a basic enigma on the brain's in-vivo mean spontaneous firing rate of a given subject. Calculating the in-vivo spontaneous firing rate is of high importance for research and for clinical purposes. In particularly, since spontaneous firing rate is affected by both the neuronal spontaneous activity (neuronal noise) and the excitability threshold, calculating the brain average spontaneous firing rate is of great medical importance that span many neuronal-malfunctioning diseases. Examples of diseases related to neuronal excitability threshold include: diabetic[47], hypertension[48], obesity[49], and examples for diseases related to neuronal noise: autism[9] and cognitive aging[10].

The in-vivo mean firing rate estimation λ, for the network of brain neurons, technically cannot be achieved by a direct invasive wet lab measurements. The firing rate is very much affected by environmental conditions, hence invasive measurements interrupt the natural spontaneous firing λ. Therefore for validation purposes we developed three alternative dry lab evaluations for in-vivo measurements, that emerge from two different approaches based on the fMRI data. All three methods show excellent agreement. Furthermore, to further support our methods, in Fig. 6 we also provide in-vitro measurements, indicating that our method could predict actual values of λ.

One of the approaches (methods II&III) that we suggest for evaluating the brain spontaneous firing rate, λ, is by analyzing the correlation coefficient, $\rho(BOLD)$, between two half's day fMRI BOLD signals. Using stochastic tools we show that the current correlation coefficient, and hence also $\rho(BOLD)$, is related to λ in both, its frequency and amplitude. Therefore we suggest here that a direct correlation between the two half's day fMRI signal, reflects the intrinsic spontaneous firing rate of the neurons. While usually the small cosine fluctuations in the current correlation coefficient are neglected or ignored, here we show that its representation as a direct correlation coefficients between two different half's day, is not merely a noise since its fluctuations can be useful for estimating λ.

Another method (method I) which we suggest concerns analyzing fMRI signal spectrum. In Supplementary Fig. S1 and Eq. (6) we describe analytically the neuronal current spectrum. We show that when f is in proximity to the value of λ, a $1/f$ behavior is represented by the current spectrum. Showing that λ has low frequency values, suggests that the spectrum at low frequencies (but not the ultra-low frequencies range) will present a near $1/f$ characteristics, as was indeed illustrated for fMRI signal[23]. Hence, based on this we develop a theory and provide the yet unknown answer to the question regarding the origin of the $1/f$ fMRI spectrum at low frequencies. We show here results, based on method-I, related to four different types of data: (i) in-vivo BOLD fMRI human data, (ii) in-vivo EEG human data, (iii) in-vitro neuronal cultures networks of animals (Fig. 6) and (iv) model simulations of Hopfield network model (Supplementary Fig. S1c, f, h). As all four show (-1) slope of *log* related to λ from very different measurements, it suggests that method-I is universal and valid for all measurements related to the neuronal current activity. Note, additionally, that the value *log* has no units, hence the measurements units are irrelevant for the slope *log*. Indeed, noise with a $1/f$ power spectral density ((-1) slope of *log*) is a common description of signals in biological (e.g., heart rate) as well as many physical systems (e.g., noise in electronic devices, gravitational-wave astronomy). In general, the origin of $1/f$ noise and its genesis are unknown, and theories regarding this noise remain questionable. Suggesting here a model that relates neurons' network with a neuronal noise input to the $1/f$ fMRI nature, could potentially be the key for understanding other $1/f$ behaviors in biological and physical systems.

Methods

Method-I: spectrum - analytical representation of the spectrum

According to Hodgkin–Huxley model (representing the current flow through the membrane lipid bilayer like a capacitor), the relation between the current, I, and the voltage, V, is: $dV_i/dt = I_i/C$, where C is the capacitance[50]. Applying this relation into Eq. (2), and considering that $\tau = \rho{\cdot}C$ for resistance ρ, yields:

$$\rho_i \cdot I_i = -V_i + \tau \cdot \sum_{j \neq i} W_{ij} R(V_j) + \tau \cdot \sigma \cdot n_i \tag{12}$$

$$I_i + V_i/\rho_i = C \cdot \sum_{j \neq i} W_{ij} R(V_j) + C \cdot \sigma \cdot n_i. \tag{13}$$

From Eq. (13) we can obtain relations between the autocorrelation of the current ($r(I,I)=E\{I(t)\cdot I(t-T)\}$), the voltage ($r(V,V)=E\{V(t)\cdot V(t-T)\}$) and the cross-correlation between the current and the voltage ($r(I,V)=E\{I(t)\cdot V(t-T)\}$), as follows

$$r(I,I)+r(V,V)/\rho^2+2\cdot r(I,V)/\rho=C^2\cdot\left(\sum_{j\neq i}W_{ij}\right)r(R,R)+C^2\cdot\sigma^2.$$

Since the power spectral density (PSD) is the Fourier transform of the autocorrelation (and the cross-correlation), applying the spectrum operator on both sides of Eq. (13), and assuming that $R(V_j)$ is an inhomogeneous Poisson process, we get the following relation to the frequency, f:

$$S+S_{VV}/\rho^2+2\cdot S_{IV}/\rho=C^2\cdot\left(\sum_{j\neq i}W_{ij}\right)^2\cdot\frac{2/\lambda}{1+(f/\lambda)^2}+C^2\cdot\sigma^2 \tag{14}$$

where S is the (absolute) PSD of the current, S_{VV} is the PSD of the voltage, and S_{IV} the PSD of the autocorrelation between the current and the voltage. Note that the firing rate $R(V_j)$ is an inhomogeneous Poisson process having autocorrelation of: $e^{-\lambda|t_2-t_1|}$, where t_1 and t_2 are the two temporal values[28]. Therefore, the PSD (Fourier transform of autocorrelation) of $R(V_j)$ is $\frac{2/\lambda}{1+(f/\lambda)^2}$.

Since, according to Hodgkin–Huxley model $V=\int I/C$[50]:

$$\begin{aligned}&S+S/(C^2\cdot f^2\cdot\rho^2)+S/(C\cdot f\cdot\rho)=C^2\cdot\left(\sum_{j\neq i}W_{ij}\right)^2\cdot\frac{2/\lambda}{1+(f/\lambda)^2}+C^2\cdot\sigma^2\\&S+S/(f^2\cdot\tau^2)+S/(f\cdot\tau)=C^2\cdot\left(\sum_{j\neq i}W_{ij}\right)^2\cdot\frac{2/\lambda}{1+(f/\lambda)^2}+C^2\cdot\sigma^2,\end{aligned} \tag{15}$$

hence, for large enough frequencies, i.e., when $f>>1/\tau$, we can approximate that:

$$\begin{aligned}&S\approx\frac{c_1}{1+(f/\lambda)^2}+c_2\\&\text{where}:\quad c_1=C^2\cdot\left(\sum_{j\neq i}W_{ij}\right)^2\cdot 2/\lambda,\quad\text{and}\quad c_2=C^2\cdot\sigma^2.\end{aligned} \tag{16}$$

From this we conclude that $c_1>>c_2$ if: (i) the neurons are connected via extensive networking connections, i.e., $\sum_{j\neq i}W_{ij}$ is relatively large (e.g., since the number of connections is large, the amount of summation $\sum_{j\neq i}$ is large); (ii) λ is small (a fraction, i.e., $\lambda<0.1$[Hz]) hence $1/\lambda$ is large; (iii) σ is small, its value is $\sim 7\cdot 10^{-3}$ V[4]. Hence, from all the above: $(\sum_{j\neq i}W_{ij})^2\cdot 2/\lambda>>\sigma^2$, and therefore, we conclude that $c_1>>c_2$. Note that concluding that $c_1>>c_2$ can be obtained also from Supplementary Fig. S2.

Note that at $f=\lambda$ the PSD gets a value of $C^2\cdot(\sum_{j\neq i}W_{ij})^2/\lambda+C^2\cdot\sigma^2$. Moreover, at $f=\infty$ the PSD is $C^2\cdot\sigma^2$. Hence, if we eliminate the PSD at $S(f=\lambda)$ from the PSD of $S(f=\infty)$ we get a value which is proportional to $(\sum_{j\neq i}W_{ij})^2$. And indeed Fig. 9 shows high correlation, ≈0.88, between neuronal network links connections and $S(f=\lambda)-S(f=\infty)$, which adds another support to our analysis.

Method-I: spectrum - extracting λ from the spectrum

From Eq. (16), we show now how to extract λ from the current spectrum S, and with neglecting c_2 ($c_1>>c_2$, see text immediately after Eq. (16)),

$$S\approx\frac{c_1}{1+(f/\lambda)^2}, \tag{17}$$

we can calculate the slope of a loglog spectrum plot, by using the following rule:

$$\frac{d\log(S)}{d\log(f)}=\frac{d\log(S)}{df}\cdot\frac{df}{d\log(f)}=\frac{d\log(S)}{df}\cdot\frac{1}{\frac{d\log(f)}{df}}=\frac{d\log(S)}{df}\cdot f. \tag{18}$$

Applying this rule, Eq. (18), for Eq. (17):

$$\log(S)=\log(c_1)-\log\left(1+\left(\frac{f}{\lambda}\right)^2\right) \tag{19}$$

$$\frac{d\log(S)}{d\log(f)}=-\frac{\left(\frac{2\cdot f}{\lambda^2}\right)}{1+\left(\frac{f}{\lambda}\right)^2}\cdot f \tag{20}$$

$$\frac{d\log(S)}{d\log(f)}=-2\cdot\frac{\left(\frac{f}{\lambda}\right)^2}{1+\left(\frac{f}{\lambda}\right)^2} \tag{21}$$

$$\left.\frac{d\log(S)}{d\log(f)}\right|_{f=\lambda}=-2\cdot\frac{1^2}{1+1^2}=-2\cdot\frac{1}{2}=-1 \tag{22}$$

Note that, in general $\frac{dlog_a(S)}{dlog_a(f)}=\frac{d\ln(S)/ln(a)}{d\ln(f)/ln(a)}=\frac{d\ln(S)}{d\ln(f)}$, therefore, same results for ln and for *log*.

Therefore, for $f=\lambda$ the slope of the loglog ($log(y)$ vs. $log(x)$) plot of the spectrum is of -1. For the case where $c_2=0$, there is no other f solution that obtain slope of -1. However, when adding constant $c_2>0$, in particularly due to noise, there will be a second solution of -1 slope, close to where the

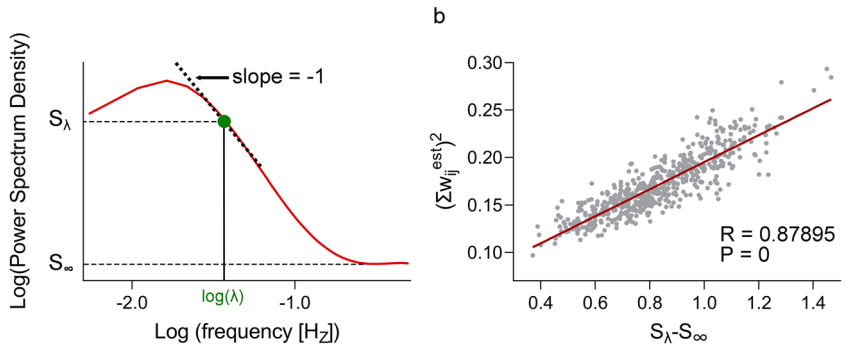

Fig. 9 | Estimating connection strength, *W*, from spectrum. a Definitions of S_λ and S_∞ as the spectrum at λ frequency ($S(f=\lambda)$) and as the spectrum at steady-state infinity frequency ($S(f=\infty)$), accordingly. **b** Correlation of ≈0.88 between the spectrum points values $S_\lambda-S_\infty$, and the connections strengths $\left(\sum_{j\neq i}W_{ij}\right)^2$. The W_{ij} are estimated from neuronal network links connections values.

PDS gets a flat c_2 value. Therefore, we always take $f = \lambda$ as the first solution (lowest f) that reach a value -1 slope within the PDS frequencies range.

Method-II & method-III: correlations - analytical representation of the correlation

Although our two approaches are distinct, their starting point is similar, as in both we use Hopfield model under the assumption that the afferent input is noise (Eq. (2)). But as we show now, the methods deviate by employing very different approaches. For example, while our first approach (method-I) considers the spectrum and assume low level of noise, in our second approach (method-II & method-III) we calculate the correlations at steady-state and assume stationarity.

Applying Eq. (2) to the i-th and the k-th neurons in the day's first half (half-1) and the day's second half (half-2):

$$\text{half}-1: \qquad \tau \cdot dV_i/dt = -V_i + \tau \cdot \sum_{j \neq i} W_{ij} R(V_j) + \tau \cdot \sigma \cdot n_i \tag{23.1}$$

$$\text{half}-2: \qquad \tau \cdot d\bar{V}_k/dt = -\bar{V}_k + \tau \cdot \sum_{j \neq k} W_{kj} R(\bar{V}_j) + \tau \cdot \sigma \cdot \bar{n}_k, \tag{23.2}$$

where the bar, e.g., $\bar{V}$, represents half-2 signal data. Note that the model parameters, such as λ, τ, W and σ, are expected to have similar values for both half-1 and half-2.

Implementing Eq. (23) in the product rule: $d(V_i \cdot \bar{V}_k)/dt = dV_i/dt \cdot \bar{V}_k + V_i \cdot d\bar{V}_k/dt$, yields that for those two neurons:

$$\begin{aligned}\tau \cdot d(V_i \cdot \bar{V}_k)/dt =& \bar{V}_k \cdot \left(-V_i + \tau \cdot \sum W_{ij} R(V_j) + \sigma \cdot n_i\right) \\ &+ V_i \cdot \left(-\bar{V}_k + \tau \cdot \sum W_{kj} R(\bar{V}_j) + \tau \cdot \sigma \cdot \bar{n}_k\right).\end{aligned}$$

Since n_i and $\bar{n}_k$ are uncorrelated with $\bar{V}_k$ and V_i (respectively), the expectation operator $E\{\}$ on both sides of Eq. (24) yields:

$$\begin{aligned}\tau \cdot d(E\{V_i \cdot \bar{V}_k\})/dt =& -2 \cdot E\{V_i \cdot \bar{V}_k\} + \tau \cdot \sum W_{ij} \cdot E\{\bar{V}_k \cdot R(V_j)\} \\ &+ \tau \cdot \sum W_{kj} E\{V_i \cdot R(\bar{V}_j)\}.\end{aligned} \tag{24}$$

Assuming that the derivative of the average product is zero, $d(E\{V_i \cdot \bar{V}_k\}) = 0$, due to stationarity, yields:

$$E\{V_i \cdot \bar{V}_k\} = \tau/2 \cdot \left(\sum_{j \neq i} W_{ij} \cdot E\{\bar{V}_k \cdot R(V_j)\} + \sum_{j \neq k} W_{kj} E\{V_i \cdot R(\bar{V}_j)\}\right). \tag{25}$$

Since $R(V)$ depends on V (voltage of half-1) and not on $\bar{V}$ (voltage of half-2), the values of $\bar{V}_i$ and $R(V_j)$ (and the values of V_i and $R(\bar{V}_j)$) are uncorrelated. Additionally, due to stationarity V and $\bar{V}$ (and $R(V)$ and $R(\bar{V})$) have similar statistics:

$$\begin{aligned}\sum_{j \neq i} W_{ij} \cdot E\{\bar{V}_k \cdot R(V_j)\} &= \sum_{j \neq k} W_{kj} E\{V_i \cdot R(\bar{V}_j)\} \\ &= \sum_{j \neq i} W_{ij} \cdot E\{V_i\} \cdot E\{R(V_j)\}\end{aligned} \tag{26}$$

hence, applying Eq. (26) into Eq. (25) yields:

$$E\{V_i \cdot \bar{V}_k\} = \tau \cdot \sum_{j \neq i} W_{ij} \cdot E\{V_i\} \cdot E\{R(V_j)\}. \tag{27}$$

$E\{V_i\}$ can be calculated from applying mean operator on both sides of Eq. (23.1), as follows:

$$\tau \cdot dE\{V_i\}/dt = -E\{V_i\} + \tau \cdot \sum_{j \neq i} W_{ij} \cdot E\{R(V_j)\} \tag{28}$$

$$E\{V_i\} = \tau \cdot \sum_{j \neq i} W_{ij} \cdot E\{R(V_j)\} \tag{29}$$

where the transition from Eq. (28) to Eq. (29) is as $dE\{V_i\}/dt = 0$ (stationarity). Implementing Eq. (29) into Eq. (27) yields:

$$E\{V_i \cdot \bar{V}_k\} = \tau^2 \cdot \left(\sum_{j \neq i} W_{ij} \cdot E\{R(V_j)\}\right)^2. \tag{30}$$

In order to calculate the current correlation between half-1 and half-2: $E\{I_i \cdot \bar{I}_k\}$, we multiply Eq. (23.1) with Eq. (23.2), and with the current-voltage relation of $I_i/C = dV_i/dt$, and we obtain (using also Eq. (25)) that:

$$\begin{aligned}\tau^2/C^2 \cdot E\{I_i \cdot \bar{I}_k\} =& E\{V_i \cdot \bar{V}_k\} + \tau^2 \cdot E\left\{\sum_{j \neq i} W_{ij} R(V_j) \cdot \sum_{j \neq k} W_{kj} R(\bar{V}_j)\right\} \\ &- 2 \cdot \tau \cdot \left(\sum_{j \neq i} W_{ij} \cdot E\{\bar{V}_k \cdot R(V_j)\} + \sum_{j \neq k} W_{kj} E\{V_i \cdot R(\bar{V}_j)\}\right)\end{aligned} \tag{31}$$

$$\begin{aligned}\tau^2/C^2 \cdot E\{I_i \cdot \bar{I}_k\} =& E\{V_i \cdot \bar{V}_k\} + \tau^2 \cdot E\left\{\sum_{j \neq i} W_{ij} R(V_j) \cdot \sum_{j \neq k} W_{kj} R(\bar{V}_j)\right\} \\ &- 2 \cdot \tau \cdot E\{V_i \cdot \bar{V}_k\}\end{aligned} \tag{32}$$

where C is the neuronal membrane capacitance. Further using Eqs. (30) on Eq. (32) yields:

$$\begin{aligned}\tau^2/C^2 \cdot E\{I_i \cdot \bar{I}_k\} =& \tau^2 \cdot E\left\{\sum_{j \neq i} W_{ij} R(V_j) \cdot \sum_{j \neq k} W_{kj} R(\bar{V}_j)\right\} \\ &- \tau^2 \cdot \left(\sum_{j \neq i} W_{ij} \cdot E\{R(V_j)\}\right)^2\end{aligned} \tag{33}$$

$$\begin{aligned}1/C^2 \cdot \sum_i \sum_k E\{I_i \cdot \bar{I}_k\} =& E\left\{\sum_i \sum_{j \neq i} W_{ij} R(V_j) \cdot \sum_k \sum_{j \neq k} W_{kj} R(\bar{V}_j)\right\} \\ &- \left(\sum_i \sum_{j \neq i} W_{ij} \cdot E\{R(V_j)\}\right)^2\end{aligned} \tag{34}$$

$$\begin{aligned}1/C^2 \cdot \sum_i \sum_k E\{I_i \cdot \bar{I}_k\} =& E\left\{\sum_i \sum_{j \neq i} W_{ij} R(V_j) \cdot \sum_k \sum_{j \neq k} W_{kj} R(\bar{V}_j)\right\} \\ &- \left(E\left\{\sum_i \sum_{j \neq i} W_{ij} \cdot R(V_j)\right\}\right)^2,\end{aligned} \tag{35}$$

which finally yields:

$$1/C^2 \cdot \sum_i \sum_k E\{I_i \cdot \bar{I}_k\} = cov\left\{\sum_i \sum_{j \neq i} W_{ij} R(V_j), \sum_k \sum_{j \neq k} W_{kj} R(\bar{V}_j)\right\} \tag{36}$$

$$1/C^2 \cdot \sum_i \sum_k E\{I_i \cdot \bar{I}_k\} = \left(\sum_i \sum_{j\neq i} W_{ij}\right)^2 cov\{R(V), R(\bar{V})\}. \quad (37)$$

From Eq. (37), and since the neurons' current I has zero mean, its correlation ($E()$) and correlation coefficient ($\rho()$) have the relation of $\left(E\{I_i \cdot \bar{I}_k\}\right)/variance\{I\} = \rho(I_i, \bar{I}_k)$, with current variance according to Eq. (51). Hence,

$$\begin{aligned} 1/C^2 \cdot \sum_i \sum_k \rho(I_i, \bar{I}_k) &= \frac{\left(\sum_i \sum_{j\neq i} W_{ij}\right)^2 cov\{R(V), R(\bar{V})\}}{variance\{I\}} \\ &= \frac{\left(\sum_i \sum_{j\neq i} W_{ij}\right)^2 cov\{R(V), R(\bar{V})\}}{\left(\sum_i \sum_{j\neq i} W_{ij}\right)^2 \cdot \lambda \cdot C^2} \end{aligned} \quad (38)$$

$$\sum_i \sum_k \rho(I_i^{\text{half}_1}, I_k^{\text{half}_2}) = \frac{cov\{R(V), R(\bar{V})\}}{\lambda}. \quad (39)$$

The firing rate of a neuron is described by an inhomogeneous Poisson process with additional slow cosine oscillations, with autocorrelation $R(V)$ as described in Eq. (5) (see also ref. 29). This yields at $\lambda \cdot (t2 - t1) \to \infty$ (where $e^{-\lambda\cdot(t2-t1)} \to 0$), as is the case for most elements of the day's two halfs, cosine oscillations around zero with frequency of λ and amplitude of p, hence applying this into Eq. (39) yields,

$$f \equiv frequence\left\{\rho(I_i^{\text{half}_1}, I_k^{\text{half}_2})\right\} = \lambda \quad (40)$$

and,

$$\sum_i \sum_k amplitude\left\{\rho(I_i^{\text{half}_1}, I_k^{\text{half}_2})\right\} = \frac{p}{\lambda}, \quad (41)$$

which is, since p is defined in Eq. (5) as a constant:

$$A \equiv amplitude\left\{\rho(I_i^{\text{half}_1}, I_k^{\text{half}_2})\right\} \propto \frac{1}{\lambda}. \quad (42)$$

Note that since for different voxels (different neurons) the value of λ could be different, we use only correlation of same voxel, i.e., instead of $\rho(I_i^{\text{half}_1}, I_k^{\text{half}_2})$ we use only same voxels (same neurons), $\rho(I_i^{\text{half}_1}, I_i^{\text{half}_2})$ as in Eqs. (9)–(11). Moreover, the fMRI data BOLD signal measures ionic currents activity[32], hence $\rho(I_i^{\text{half}_1}, I_i^{\text{half}_2})$ can be obtain from the fMRI BOLD signal correlation-coefficient, which we name $\rho(BOLD)$. The main conclusion from Eqs. (40) and (42) is that an FFT analysis (frequency and amplitude) of $\rho(BOLD)$ can be used to calculate λ.

Method-II & method-III: correlations - calculating current variance

Applying sum, square and mean operators, $E\{(\sum_i)^2\}$, in Eq. (1) yields:

$$\begin{aligned} \tau^2/C^2 \cdot E\left\{\left(\sum_i I_i\right)^2\right\} &= E\left\{\left(\sum_i V_i\right)^2\right\} - \tau \cdot \sum_i \sum_{j\neq i} W_{ij} E\{V_i \cdot R(V_j)\} \\ &+ \tau^2 \cdot \left(\sum_i \sum_{j\neq i} W_{ij}\right)^2 E\{R(V_j) \cdot R(V_i)\} + N\tau^2 \cdot \sigma^2. \end{aligned} \quad (43)$$

Since V_i and $R(V_j)$ are uncorrelated for $i \neq j$:

$$\begin{aligned} \tau^2/C^2 \cdot E\left\{\left(\sum_i I_i\right)^2\right\} &= E\left\{\left(\sum_i V_i\right)^2\right\} - \tau \cdot \sum_i \sum_{j\neq i} W_{ij} E\{V_i\} \cdot E\{R(V_j)\} \\ &+ \tau^2 \cdot \left(\sum_i \sum_{j\neq i} W_{ij}\right)^2 E\{R(V_j) \cdot R(V_i)\} + N\tau^2 \cdot \sigma^2 \end{aligned} \quad (44)$$

$$\begin{aligned} \tau^2/C^2 \cdot E\left\{\left(\sum_i I_i\right)^2\right\} &= E\left\{\left(\sum_i V_i\right)^2\right\} - \tau \cdot \sum_{j\neq i} W_{ij} E\{V_i\} \cdot \lambda \\ &+ \tau^2 \cdot \left(\sum_i \sum_{j\neq i} W_{ij}\right)^2 E\{R(V_j) \cdot R(V_i)\} + N\tau^2 \cdot \sigma^2. \end{aligned} \quad (45)$$

Note that for the variance calculations we use $t = 0$, hence the R probability is an inhomogeneous Poisson process with λ mean and variance. Further using Eq. (29) yields:

$$\begin{aligned} \tau^2/C^2 \cdot E\left\{\left(\sum_i I_i\right)^2\right\} &= E\left\{\left(\sum_i V_i\right)^2\right\} - \tau^2 \cdot \left(\sum_i \sum_{j\neq i} W_{ij}\right)^2 \cdot \lambda^2 \\ &+ \tau^2 \cdot \left(\sum_i \sum_{j\neq i} W_{ij}\right)^2 E\{R(V_j) \cdot R(V_i)\} + N\tau^2 \cdot \sigma^2 \end{aligned} \quad (46)$$

$$\begin{aligned} \tau^2/C^2 \cdot E\left\{\left(\sum_i I_i\right)^2\right\} &= C^2 \int \sum_i \sum_j E\{I_i \cdot I_j\} - \tau^2 \cdot \left(\sum_i \sum_{j\neq i} W_{ij}\right)^2 \cdot \lambda^2 \\ &+ \tau^2 \cdot \left(\sum_i \sum_{j\neq i} W_{ij}\right)^2 E\{R(V_j) \cdot R(V_i)\} + N\tau^2 \cdot \sigma^2. \end{aligned} \quad (47)$$

Considering that physiologically $C << 1$, we get after neglecting C^2 value:

$$\begin{aligned} \tau^2/C^2 \cdot E\left\{\left(\sum_i I_i\right)^2\right\} &= -\tau^2 \cdot \left(\sum_i \sum_{j\neq i} W_{ij}\right)^2 \cdot \lambda^2 \\ &+ \tau^2 \cdot \left(\sum_i \sum_{j\neq i} W_{ij}\right)^2 E\{R(V_j) \cdot R(V_i)\} + N\tau^2 \cdot \sigma^2, \end{aligned} \quad (48)$$

and with $E\{R^2\} = variance\{R\} + (E\{R\})^2 = \lambda + \lambda^2$, it is obtained that:

$$\begin{aligned} \tau^2/C^2 \cdot E\left\{\left(\sum_i I_i\right)^2\right\} &= -\tau^2 \cdot \left(\sum_i \sum_{j\neq i} W_{ij}\right)^2 \cdot \lambda^2 \\ &+ \tau^2 \cdot \left(\sum_i \sum_{j\neq i} W_{ij}\right)^2 \cdot (\lambda^2 + \lambda) + N\tau^2 \cdot \sigma^2. \end{aligned} \quad (49)$$

For small λ values (as $\lambda < 0.1[Hz]$), we neglect λ^2:

$$\tau^2/C^2 \cdot E\left\{\left(\sum_i I_i\right)^2\right\} = \tau^2 \cdot \left(\sum_i \sum_{j\neq i} W_{ij}\right)^2 \cdot \lambda + N\tau^2 \cdot \sigma^2. \quad (50)$$

The term $N \cdot \sigma^2$ can be neglected relatively to $\left(\sum_i \sum_{j\neq i} W_{ij}\right)^2$, this since $\sigma << \sum_{j\neq i} W_{ij}$ (same reason that $c_1 >> c_2$, see text immediately after Eq. (16)),

and since $N << \left(\sum_i \sum_{j\neq i}\right)^2 \approx N^4$:

$$variance\left\{\sum_i I_i\right\} = \left(\sum_i \sum_{j\neq i} W_{ij}\right)^2 \cdot \lambda \cdot C^2. \quad (51)$$

Note that $E\{(\sum_i I_i)^2\} = variance\{I\}$ since the avarage value of the current is zero, $E\{I\} = 0$.

Simulating spontaneous firing rate

The simulations we performed in Supplementary Fig. S1c, f, have been obtained using the following equations:

$$\tau \cdot dV_i/dt = -V_i + \tau \cdot \sum_{j\neq i} W_{ij} R(V_j) + \tau \cdot \sigma \cdot n_i \quad (52)$$

with

$$R(V_j) = \frac{1}{\Delta t} = 1/(t_2 - t_1), \quad (53)$$

where $\Delta t = t_2 - t_1$ is the time gap between the two latest spikes of the spikes train of the simulation. Therefore, the Δt in Eq. (53) represents the time interval between two consecutive voltage action potential peaks above threshold (see Fig. 1a). Eq. (53) represents $R(V_j)$ the firing rate of the j-th neuron, which is instead of the deterministic function of the voltage (such as hyperbolic tangent[11,25], or logarithmic function[51,52]). Using Eq. (53) platform, the firing rate $R(V_j)$ describes an inhomogeneous Poisson process of the neuronal spikes without external stimulation[26,27].

Note that Eq. (52) represents voltage, where the spikes train is obtained using a specific thresholds, as shown in Fig. 1a. In our simulation, it is important to calculate the present spikes train of each simulation time, since $R(V_j) = 1/\Delta t$ where Δt is the time gap between two latest spikes train. Specifically,

$$V_i(t_k) = V_i(t_{k-1}) + (dt/\tau) \cdot \left(-V_i + \tau \cdot \sum_{j\neq i} W_{ij} R_{t_k}(V_j) + \tau \cdot \sigma \cdot n_i\right) \quad (54)$$

$$\text{spike apears when } V_i(t_k) > \text{threshold} \quad (55)$$

$$R_{t_k} = 1/\Delta t, \text{ where } \Delta t \text{ is the time gap between two latest spikes (up to the time } t_k). \quad (56)$$

Figure 1a, shows an example of a produced spikes train vs. voltage from our actual simulation. Importantly, note that in the simulations, λ is not a predetermined variable, but rather is calculated from the simulation. By changing the simulations variables σ and/or the threshold, the lambda is changed.

The data - statistics and reproducibility

Data has been collected from the Human Connectome Project (HCP) Data project[53]. The data includes 994 healthy, young adult subjects with records of 14.4 [min] length. For each participant, resting state fMRI was measured during two different days (Day-1, and Day-2). In addition, each participant underwent serious of brain task performances.

Please refer to "HCP_S1200_DataDictionary_April" in "https://wiki.humanconnectome.org" for the chart specifying all the measured brain task performances.

All our figures, except Fig. 2b (which includes all $N = 767$ subjects), were obtained for $N = 710$ subjects, as they show consistency in the λ values in both days (less than 40% differences, i.e., $0.6 < day1/day2 < (1/0.6)$). Future work with better consistency (hence, including more subjects), could use data with longer time records, better resolution or includes records of more days.

For preprocessing purpose, we use the outputs of the minimal preprocessing pipelines, developed by members of the WU-Minn HCP in collaboration with members of the MGH/UCLA HCP[54]. Moreover, in order to separate the whole brain into a set of regions, we used the multimodal parcellation atlas (HCP MMP atlas)[55]. This HCP MMP atlas includes 180 regions of interest (voxels) in each hemisphere.

Technical notes and differences between method-I and methods-II&III

The source codes to obtain methods I-III can be found in Supplementary Materials.

For method-I, in order to get a smooth spectrum, we calculate an averaged spectrum for each participant based on all 360 voxels (except the 21 Limbic system voxels) as shown in Supplementary Fig. S2. In order to get λ for each functional systems, we calculate one averaged spectrum for a participant from all voxels within the specific brain's functional system. Each voxel's spectrum is obtained from averaging the spectrum from 300 points (3.6[min]) segments, with 150 points (1.8 min) overlap. Each segment used a Bartlett–Hanning window calculated from 10 smaller segments without overlaps. For the averaged smooth spectrum, we fit a 6th polynomial, and from this polynomial we analytically get the derivative from which we calculated the first value above 0.03 Hz where the slope is -1, this is the frequency value where λ is detected. Note that we find this point analytically, i.e., we first fit a 6-degree polynomial to the loglog spectrum and we analyze where the derivative of this analytical polynomial equation is -1.

For methods-II&III we calculate the auto-correlation between two half's day, $\rho(BOLD)$, using sliding window of size 2.88 min. We calculate the correlation of this fixed window from half-1 on half-2 with time shifts of one data (0.72 s) increments. The value of f and A are obtained from the maximal correlation value that is also a local maximum for frequencies above 0.02 (in accordance with method-I). Repeating this process, we obtain correlations for all possible locations of such 2.88 min windows from half-1. This yields value of f and A^2 for each of voxel, from all possible windows, and therefore to get a single averaged value of spontaneous firing rate estimation for a voxel we averaged all f and A^2 from all the possible windows correlations.

In all our methods, we calculate mean spontaneous firing rate estimation in both days separately, and than average the values from both days for each participant. Two main technical differences are noted between our two approach: (i) Since for the Limbic system we find high c_2 (Eq. (17)) and no -1 slope in the range, we conclude that only methods-II&III can be used to estimate spontaneous firing rate of the Limbic system. (ii) Since for method-I we need a smooth spectrum, we averaged all voxels' spectrums for one participant. Therefore, λ can be calculated for an area rather than for an individual voxel. Nevertheless, methods-II&III can be used to estimate spontaneous firing rate of a voxel. Hence methods-II&III have higher spatial resolution (therefore, Fig. 5c is obtained using method-III), while method-I might have higher accuracy due to the smoothening. Note that if more data is provided (longer data or additional days measured), method-I could present higher spatial resolution, since for more data for a participant the spectrum is more smooth.

Reporting summary

Further information on research design is available in the Nature Portfolio Reporting Summary linked to this article.

Data availability

Dataset of fMRI Data has been collected from the Human Connectome Project (HCP) Data project, which can be find in ref. 53. The EEG data can be found in ref. 36. For the animal experiments of isolated leech ganglia and hippocampal cultures from Wistar rats, the data are available from ref. 2 (see Fig. 8 in ref. 2). All other data are available from the corresponding authors on reasonable request. The source data behind the graphs in the paper can be found on our paper supplementary in Supplementary-Data-1.

Code availability

Oue codes used for analysis are available on our paper supplementary under the file name Supplementary-Software-1. Those codes are designed for the databases using MATLAB software.

Received: 7 October 2024; Accepted: 5 August 2025;
Published online: 26 August 2025

References

1. Raichle, M. E. The brain's dark energy. *Science* **314**, 1249–1250 (2006).
2. Mazzoni, A. et al. On the dynamics of the spontaneous activity in neuronal networks. *PloS One* **2**, e439 (2007).
3. Dvir, H. et al. Neuronal noise as an origin of sleep arousals and its role in sudden infant death syndrome. *Sci. Adv.* **4**, eaar6277 (2018).
4. Dvir, H. et al. A biased diffusion approach to sleep dynamics reveals neuronal characteristics. *Biophys. J.* **117**, 987–997 (2019).
5. Dvir, H. & Zlochiver, S. Interbeat interval modulation in the sinoatrial node as a result of membrane current stochasticity—a theoretical and numerical study. *Biophys. J.* **108**, 1281–1292 (2015).
6. Dvir, H. & Zlochiver, S. Stochastic cardiac pacing increases ventricular electrical stability—a computational study. *Biophys. J.* **105**, 533–542 (2013).
7. Sanhedrai, H., Havlin, S. & Dvir, H. Mechanistic description of spontaneous loss of memory persistent activity based on neuronal synaptic strength. *Heliyon* **10**, e23949 (2024).
8. Howarth, C., Gleeson, P. & Attwell, D. Updated energy budgets for neural computation in the neocortex and cerebellum. *J. Cereb. Blood Flow. Metab.* **32**, 1222–1232 (2012).
9. Weinger, P. M., Zemon, V., Soorya, L. & Gordon, J. Low-contrast response deficits and increased neural noise in children with autism spectrum disorder. *Neuropsychologia* **63**, 10–18 (2014).
10. Li, S.-C., Lindenberger, U. & Sikström, S. Aging cognition: from neuromodulation to representation. *Trends Cogn. Sci.* **5**, 479–486 (2001).
11. Hopfield, J. J. Neurons with graded response have collective computational properties like those of two-state neurons. *Proc. Natl Acad. Sci.* **81**, 3088–3092 (1984).
12. Gosak, M., Milojević, M., Duh, M., Skok, K. & Perc, M. Networks behind the morphology and structural design of living systems. *Phys. Life Rev.* **41**, 1–21 (2022).
13. Artime, O. et al. Robustness and resilience of complex networks. *Nat. Rev. Phys.* **6**, 114–131 (2024).
14. De La Prida, L. M. & Gal, B. Synaptic contributions to focal and widespread spatiotemporal dynamics in the isolated rat subiculum in vitro. *J. Neurosci.* **24**, 5525–5536 (2004).
15. Uusisaari, M., Obata, K. & Knopfel, T. Morphological and electrophysiological properties of GABAergic and non-GABAergic cells in the deep cerebellar nuclei. *J. Neurophysiol.* **97**, 901–911 (2007).
16. Ben-Naim, E., Frauenfelder, H. & Toroczkai, Z. *Complex networks*, 650 (Springer Science & Business Media, 2004).
17. Gosak, M. et al. Network science of biological systems at different scales: a review. *Phys. Life Rev.* **24**, 118–135 (2018).
18. Solomon, S. & Shir, B. Complexity; a science at 30. *Europhys. N.* **34**, 54–57 (2003).
19. Xu, X.-J., Zhang, X. & Mendes, J. Impacts of preference and geography on epidemic spreading. *Phys. Rev. E* **76**, 056109 (2007).
20. Louzada, V. H., Araújo, N. A., Andrade, J. S. & Herrmann, H. J. Breathing synchronization in interconnected networks. *Sci. Rep.* **3**, 1–5 (2013).
21. Arenas, A., Díaz-Guilera, A., Kurths, J., Moreno, Y. & Zhou, C. Synchronization in complex networks. *Phys. Rep.* **469**, 93–153 (2008).
22. Barabási, A.-L., Gulbahce, N. & Loscalzo, J. Network medicine: a network-based approach to human disease. *Nat. Rev. Genet.* **12**, 56–68 (2011).
23. Fox, M. D. & Raichle, M. E. Spontaneous fluctuations in brain activity observed with functional magnetic resonance imaging. *Nat. Rev. Neurosci.* **8**, 700–711 (2007).
24. Orlandi, J. G., Soriano, J., Alvarez-Lacalle, E., Teller, S. & Casademunt, J. Noise focusing and the emergence of coherent activity in neuronal cultures. *Nat. Phys.* **9**, 582–590 (2013).
25. Lansner, A. Associative memory models: from the cell-assembly theory to biophysically detailed cortex simulations. *Trends Neurosci.* **32**, 178–186 (2009).
26. Van Etten, W. C. *Introduction to random signals and noise* (John Wiley & Sons, 2006).
27. Gabbiani, F. & Cox, S. J. *Mathematics for neuroscientists* (Academic Press, 2017).
28. Stark, H. & Woods, J. W. *Probability, statistics, and random variables for engineers* (Pearson Education Inc., 2012).
29. Zeraati, R., Engel, T. A. & Levina, A. A flexible Bayesian framework for unbiased estimation of timescales. *Nat. Comput. Sci.* **2**, 193–204 (2022).
30. Kelly, R. C., Smith, M. A., Kass, R. E. & Lee, T. S. Local field potentials indicate network state and account for neuronal response variability. *J. Comput. Neurosci.* **29**, 567–579 (2010).
31. Ecker, A. S. et al. State dependence of noise correlations in macaque primary visual cortex. *Neuron* **82**, 235–248 (2014).
32. Bianciardi, M., Di Russo, F., Aprile, T., Maraviglia, B. & Hagberg, G. E. Combination of BOLD-fMRI and VEP recordings for spin-echo MRI detection of primary magnetic effects caused by neuronal currents. *Magn. Reson. imaging* **22**, 1429–1440 (2004).
33. Gao, Z.-K., Small, M. & Kurths, J. Complex network analysis of time series. *EPL Europhys. Lett.* **116**, 50001 (2017).
34. Wang, Q., Chen, G. & Perc, M. Synchronous bursts on scale-free neuronal networks with attractive and repulsive coupling. *PLoS One* **6**, e15851 (2011).
35. Boccaletti, S., Pisarchik, A. N., Del Genio, C. I. & Amann, A. *Synchronization: from coupled systems to complex networks* (Cambridge University Press, 2018).
36. Gajewski, P. D. et al. Impact of biological and lifestyle factors on cognitive aging and work ability in the Dortmund Vital Study: protocol of an interdisciplinary, cross-sectional, and longitudinal study. *JMIR Res. Protoc.* **11**, e32352 (2022).
37. Faisal, A. A., Selen, L. P. & Wolpert, D. M. Noise in the nervous system. *Nat. Rev. Neurosci.* **9**, 292–303 (2008).
38. Heck, A. et al. Converging genetic and functional brain imaging evidence links neuronal excitability to working memory, psychiatric disease, and brain activity. *Neuron* **81**, 1203–1213 (2014).
39. Goldman-Rakic, P. S. Regional and cellular fractionation of working memory. *Proc. Natl Acad. Sci.* **93**, 13473–13480 (1996).
40. Hoegl, T. et al. Time course analysis of motor excitability in a response inhibition task according to the level of hyperactivity and impulsivity in children with ADHD. *PLoS One* **7**, e46066 (2012).
41. Lu, Z.-L. & Dosher, B. A. External noise distinguishes attention mechanisms. *Vis. Res.* **38**, 1183–1198 (1998).
42. Bolger, D., Coull, J. T. & Schön, D. Metrical rhythm implicitly orients attention in time as indexed by improved target detection and left inferior parietal activation. *J. Cogn. Neurosci.* **26**, 593–605 (2014).
43. Biasiucci, A., Franceschiello, B. & Murray, M. M. Electroencephalography. *Curr. Biol.* **29**, R80–R85 (2019).
44. Linkenkaer-Hansen, K., Nikouline, V. V., Palva, J. M. & Ilmoniemi, R. J. Long-range temporal correlations and scaling behavior in human brain oscillations. *J. Neurosci.* **21**, 1370–1377 (2001).
45. Schreckenberger, M. et al. The thalamus as the generator and modulator of EEG alpha rhythm: a combined PET/EEG study with lorazepam challenge in humans. *Neuroimage* **22**, 637–644 (2004).
46. Grodd, W., Kumar, V. J., Schüz, A., Lindig, T. & Scheffler, K. The anterior and medial thalamic nuclei and the human limbic system:

tracing the structural connectivity using diffusion-weighted imaging. *Sci. Rep.* **10**, 10957 (2020).
47. Krishnan, A. V. & Kiernan, M. C. Altered nerve excitability properties in established diabetic neuropathy. *Brain* **128**, 1178–1187 (2005).
48. Moraes, D. J., Machado, B. H. & Paton, J. F. Specific respiratory neuron types have increased excitability that drive presympathetic neurones in neurogenic hypertension. *Hypertension* **63**, 1309–1318 (2014).
49. Harvey, J. Leptin regulation of neuronal excitability and cognitive function. *Curr. Opin. Pharmacol.* **7**, 643–647 (2007).
50. Hille, B. *Ion channels of excitable membranes*, 507 (Sinauer, 2001).
51. Durstewitz, D., Seamans, J. K. & Sejnowski, T. J. Neurocomputational models of working memory. *Nat. Neurosci.* **3**, 1184–1191 (2000).
52. Amit, D. J. & Brunel, N. Learning internal representations in an attractor neural network with analogue neurons. *Netw. Comput. Neural Syst.* **6**, 359–388 (1995).
53. Van Essen, D. C. et al. The WU-Minn human connectome project: an overview. *Neuroimage* **80**, 62–79 (2013).
54. Glasser, M. F. et al. The minimal preprocessing pipelines for the human connectome project. *Neuroimage* **80**, 105–124 (2013).
55. Glasser, M. F. et al. A multi-modal parcellation of human cerebral cortex. *Nature* **536**, 171–178 (2016).

Acknowledgements

We thank the Israel Ministry of Innovation, Science & Technology (grant number 01017980), the Israel Science Foundation (grant numbers 2830/23, 201/25), the Binational Israel-China Science Foundation (grant number 3132/19), the European Union under the Horizon Europe grant OMINO (grant number 101086321).

Author contributions

H.D. conceived the study, developed the mathematical frameworks, wrote the manuscript, analyzed data, obtained and designed the figures, discussed the manuscript, performed the research; S.G. analyzed data, discussed the manuscript, gave inputs on the study, achieved the data, obtained and designed the figures, reviewed the manuscript, performed the research; R.K. and D.L. gave notes on the paper; S.H. reviewed and edited the manuscript, gave inputs on the research, discussed the manuscript, supervised the project.

Competing interests

The authors declare no competing interests.

Additional information

Supplementary information The online version contains supplementary material available at https://doi.org/10.1038/s42003-025-08667-8.

Correspondence and requests for materials should be addressed to Hila Dvir or Shu Guo.

Peer review information *Communications Biology* thanks the anonymous reviewers for their contribution to the peer review of this work. Primary Handling Editor: Benjamin Bessieres.